

**REMOVAL OF DYE USING POWDERED
ACTIVATED CARBON COATED ON
POLYURETHANE FOAM**

EILEEN KI LI SZE

UNIVERSITI TUNKU ABDUL RAHMAN

**REMOVAL OF DYE USING POWDERED ACTIVATED CARBON
COATED ON POLYURETHANE FOAM**

EILEEN KI LI SZE


**A project report submitted in partial fulfilment of the
requirements for the award of Bachelor of Chemical
Engineering with Honours**

**Lee Kong Chian Faculty of Engineering and Science
Universiti Tunku Abdul Rahman**

May 2023

DECLARATION

I hereby declare that this project report is based on my original work except for citations and quotations which have been duly acknowledged. I also declare that it has not been previously and concurrently submitted for any other degree or award at UTAR or other institutions.

Signature : 

Name : Eileen Ki Li Sze

ID No. : 1801584

Date : 20th May 2023

APPROVAL FOR SUBMISSION

I certify that this project report entitled “**REMOVAL OF DYE USING POWDERED ACTIVATED CARBON COATED ON POLYURETHANE FOAM**” was prepared by **EILEEN KI LI SZE** has met the required standard for submission in partial fulfilment of the requirements for the award of Bachelor of Chemical Engineering with Honours at Universiti Tunku Abdul Rahman.

Approved by,

Signature :  _____

Supervisor : Dr. Sim Lan Ching

Date : 20th May 2023

Signature : _____

Co-Supervisor : _____

Date : _____

The copyright of this report belongs to the author under the terms of the copyright Act 1987 as qualified by Intellectual Property Policy of Universiti Tunku Abdul Rahman. Due acknowledgement shall always be made of the use of any material contained in, or derived from, this report.

© 2023, EILEEN KI LI SZE. All right reserved.

ACKNOWLEDGEMENTS

I would like to thank everyone who had contributed to the successful completion of this project. I would like to express my gratitude to my research supervisor, Dr. Sim Lan Ching for her invaluable advice, guidance and her enormous patience throughout the development of the research.

In addition, I would also like to express my gratitude to my loving parents and friends who had helped and given me encouragement during my hardest times. Without them, I would not be able to resolve my problems which I had encountered during my research work and report writing.

ABSTRACT

This study investigates the potential use of powdered activated carbon coated on polyurethane foam (PAC/PUF) as an adsorbent to remove Congo Red dye from synthetic aqueous solution. The adsorbent is crucial to the removal of Congo Red as the dye is known to be carcinogenic and mutagenic in nature. A little concentration of less than 1 part per million (ppm) is enough to pollute the water bodies, prevent photosynthesis and affect aquatic growth. The PAC/PUF was synthesized by the dip-coating method and characterized by scanning electron microscopy with energy dispersive X-ray (SEM-EDX), X-ray diffraction (XRD), and Fourier transform infrared (FTIR) spectroscopy. The findings indicated that PAC was effectively coated on the dodecahedral skeleton surface of the PUF. Response surface methodology based on central composite design was used to optimize the effect of different adsorption parameters such as the pH, contact time, and initial concentration of dye. The optimal adsorption efficiency of Congo Red was 89.86 % at a pH of 3.854, contact time of 137.55 min, and initial concentration of dye at 33.566 mg/L. Removal of dye in low pH was better than in high pH solutions. The efficiency of adsorption improved with longer contact time but declined with increasing initial dye concentration. The kinetic studies indicated that the adsorption kinetic of Congo Red onto PAC/PUF followed the pseudo-second order kinetic model. The equilibrium data also revealed that the Langmuir isotherm model was more suitable for describing the dye adsorption. According to EDX, XRD, and FTIR characterizations, Congo Red was successfully adsorbed by PAC/PUF, suggesting both electrostatic and physical interactions between the dye and the PAC/PUF surface functional groups. Lastly, a comparison among PAC/PUF, PAC, and PUF adsorptions showed that PAC/PUF obtained the highest adsorption efficiency of Congo Red, further proved the potential use of PAC/PUF in adsorbing Congo Red.

TABLE OF CONTENTS

DECLARATION		i
APPROVAL FOR SUBMISSION		ii
ACKNOWLEDGEMENTS		iv
ABSTRACT		v
TABLE OF CONTENTS		vi
LIST OF TABLES		ix
LIST OF FIGURES		xi
LIST OF SYMBOLS / ABBREVIATIONS		xiii
LIST OF APPENDICES		xv
CHAPTER		
1	INTRODUCTION	1
1.1	General Introduction	1
1.2	Importance of the Study	3
1.3	Problem Statement	4
1.4	Aim and Objectives	5
1.5	Scope and Limitation of the Study	5
1.6	Contribution of the Study	6
1.7	Outline of the Report	6
2	LITERATURE REVIEW	7
2.1	Introduction of Dyes	7
2.2	Sources of Dyes	8
2.3	Environmental Impact of Dyes	9
2.4	Treatment Techniques	10
2.4.1	Adsorption	12
2.5	Types of Adsorbents	13
2.5.1	Activated Carbon	13
2.5.2	Zeolites	14
2.5.3	Silica Gel	15

	2.5.4 Alumina	16
2.6	Polyurethane Foam	20
2.7	Synthesis of Adsorbent	21
	2.7.1 Dip-Coating	21
	2.7.2 Impregnation	21
2.8	Composite Adsorbents Applications	22
2.9	Factors Affecting Adsorption Efficiency	22
	2.9.1 Initial Concentration of Dye	23
	2.9.2 pH	25
	2.9.3 Contact Time	27
2.10	Design of Experiment	29
2.11	Characterization of PAC/PUF	30
	2.11.1 Scanning Electron Microscopy with Energy Dispersive X-Ray (SEM-EDX)	31
	2.11.2 X-Ray Diffraction (XRD)	32
	2.11.3 Fourier-Transform Infrared (FTIR) Spectroscopy	33
2.12	Adsorption Model	34
	2.12.1 Langmuir Isotherm Model	35
	2.12.2 Freundlich Isotherm Model	36
	2.12.3 Pseudo First-Order Kinetic Model	37
	2.12.4 Pseudo Second-Order Kinetic Model	37
3	METHODOLOGY AND WORK PLAN	39
	3.1 Introduction	39
	3.2 Materials and Chemicals	39
	3.3 Equipment	40
	3.4 Methodology Flow Chart	40
	3.5 Synthesis of PAC/PUF Adsorbent	41
	3.6 Preparation of Congo Red Stock Solution	42
	3.7 Characterisation of Adsorbents	42
	3.8 Adsorption Experiment	43
	3.9 Design of Experiment	44
	3.10 Determination of Adsorption Efficiency and Capacity	45

3.11	Isotherm and Kinetic Study	46
3.11.1	Adsorption Isotherm	47
3.11.2	Adsorption Kinetic	47
4	RESULTS AND DISCUSSION	48
4.1	Characterization	48
4.1.1	SEM-EDX	48
4.1.2	XRD	52
4.1.3	FTIR	53
4.1.4	Point of Zero Charge	55
4.2	Statistical Analysis and Optimization Study	56
4.2.1	Regression Analysis	56
4.2.2	Response Surface Analysis	63
4.2.3	Optimization and Model Validation	66
4.3	Adsorption Model	68
4.3.1	Kinetic Model	68
4.3.2	Isotherm Model	71
4.4	Comparison of Various Adsorbents	74
5	CONCLUSIONS AND RECOMMENDATIONS	75
5.1	Conclusions	75
5.2	Recommendations for Future Work	76
	REFERENCES	78
	APPENDICES	93

LIST OF TABLES

Table 1.1:	Properties of Congo Red Dye (PubChem, 2023).	2
Table 2.1:	Range of Dyes Classes (Benkhaya, M' rabet and el Harfi, 2020).	7
Table 2.2:	Disadvantage of Conventional Treatment Technique.	11
Table 2.3:	Summary of Various Adsorbents.	17
Table 2.4:	Range of Initial Concentration of Dye Reported by Other Studies.	24
Table 2.5:	Range of pH Reported by Other Studies.	26
Table 2.6:	Range of Contact Time Reported by Other Studies.	28
Table 2.7:	Typical Wavenumber for Different Functional Groups (Mohamed et al., 2017).	34
Table 3.1:	Specifications of Materials and Chemicals Used.	39
Table 3.2:	Instruments Used in the Experiment.	40
Table 3.3:	Range of Actual Values and Coded Levels for Each Variable.	44
Table 3.4:	Experimental Design Matrix of CCD Coded Variables.	44
Table 3.5:	Isotherm and Kinetic Adsorption Models.	46
Table 4.1:	EDX Results of Various Adsorbents.	51
Table 4.2:	Adsorption Efficiency Based on Experimental Design Matrix.	57
Table 4.3:	ANOVA Results for Congo Red Adsorption Efficiency.	60
Table 4.4:	Experimental Versus Predicted Values of the Adsorption Efficiency of Congo Red.	67
Table 4.5:	Data for Pseudo-First and Pseudo-Second Order Modelling.	69
Table 4.6:	Parameters and Constants for Kinetic Modelling.	70
Table 4.7:	Data for Langmuir and Freundlich Modelling.	72

Table 4.8: Parameters and Constants for Isotherm Modelling.

73

LIST OF FIGURES

Figure 2.1:	Sources of Dyes (Katheresan, Kansedo and Lau, 2018).	9
Figure 2.2:	Response Plots of Adsorption of Congo Red (a) 3D Surface Response Plots and (b) 2D Contour Plots (Van Pham et al., 2019).	30
Figure 2.3:	SEM Images of AC/PUF (a) Before Adsorption and (b) After Adsorption Experiment (Wu et al., 2019).	31
Figure 2.4:	EDX Spectrum of DAC/PUF (a) Before Adsorption and (b) After Adsorption Experiment (Mallakpour and Behranvand, 2021).	32
Figure 2.5:	FTIR Spectrum of Congo Red and Methylene Blue Adsorptions by Walnut Shell Activated Carbon (Li et al., 2020).	33
Figure 2.6:	FTIR Spectrum of PUF Modified with Recycle PUF Polyol (Kraitape and Thongpin, 2016).	34
Figure 3.1:	Methodology Flow Chart	41
Figure 3.2:	Synthesis of PAC/PUF.	42
Figure 3.3:	Congo Red Solutions at Different Concentrations and pH	43
Figure 4.1:	SEM Images of Blank PUF (a, b), PAC/PUF Before Adsorption (c,d) and PAC/PUF After Adsorption (e,f) with Different Magnifications.	50
Figure 4.2:	XRD Results of Blank PUF and PAC/PUF Before and After Adsorption.	53
Figure 4.3:	FTIR Spectra of Congo Red.	54
Figure 4.4:	FTIR Spectra of PUF.	55
Figure 4.5:	FTIR Spectra of PAC/PUF Before Adsorption and PAC/PUF After Adsorption.	55
Figure 4.6:	Point of Zero Charge of PAC/PUF.	56
Figure 4.7:	Predicted and Actual Values for Adsorption Efficiency of Congo Red.	62
Figure 4.8:	Perturbation Plot of Three Independent Variables Affecting Adsorption Efficiency of Congo Red (A = pH;	

	B = Contact Time; C = Initial Concentration of Congo Red).	63
Figure 4.9:	Effects of Three Independent Variables Affecting Adsorption Efficiency of Congo Red at Fixed (a) Initial Concentration of 40 mg/L; (b) Contact Time of 120 min; (c) pH of 3.5.	64
Figure 4.10:	Adsorption Kinetic Plot of Congo Red on PAC/PUF at Fixed Conditions (pH = 3.854 and Initial Concentration of Dye = 33.566 mg/L).	69
Figure 4.11:	Pseudo-First Order Kinetic Plot.	70
Figure 4.12:	Pseudo-Second Order Kinetic Plot.	70
Figure 4.13:	Langmuir Isotherm Plot for Adsorption of Congo Red.	73
Figure 4.14:	Freundlich Isotherm Plot for Adsorption of Congo Red.	73
Figure 4.15:	Adsorption Efficiency by Various Adsorbents.	74

LIST OF SYMBOLS / ABBREVIATIONS

b	adsorption capacity, L/mg
C_e	adsorbate concentration at equilibrium, mg/L
C_f	final concentration of dye, mg/L
C_o	initial concentration of dye, mg/L
d	distance between two lattice planes, m
k_1	first order rate constant, min^{-1}
k_2	second order rate constant, min^{-1}
K_L	Langmuir constant, L/mg
n	adsorption intensity
q_e	amount of dye adsorbed at equilibrium, mg/g
q_o	amount of dye adsorbed, mg/g
q_t	amount of dye on PAC/PUF at time t, mg/g
R_L	separation factor
t	time, min
V	volume of dye solution, L
w	mass of PAC/PUF, g
θ	angle between incident X-ray and normal to reflecting plane
λ	wavelength of X-ray, m
η	order of reflection
AC/PUF	activated carbon on polyurethane foam
ANOVA	analysis of variance
AOP	advanced oxidation process
BAC	biologically active granular activated carbon
BF	basic fuchsin
COD	chemical oxygen demand
CR	congo red
CV	crystal violet
CCD	central composite design
DAC/PUF	disc-derived activated carbon on polyurethane foam

DEES	diesel exhaust emission soot
DHS	down-flow hanging sponge
DNCC	dinitro calix-4-arena cage
FE-SEM	field emission scanning electron microscopy
FTIR	Fourier Transform Infrared
GAC	granular activated carbon
GWAC	grass-derived activated carbon
HCl	hydrochloric acid
IR	infrared
MB	methylene blue
MG	malachite green
MO	methyl orange
MR	methyl red
NaCl	sodium chloride
NaOH	sodium hydroxide
PAC	powdered activated carbon
PAC/PUF	powdered activated carbon coated on polyurethane foam
PFO	pseudo first-order
pH _{pzc}	point of zero charge pH
PSO	pseudo second-order
PTFAC	palm tree fiber-derived activated carbon
RhB	rhodamine B
RMAC	rosemary-derived activated carbon
RO5	reactive orange 5
RO16	reactive orange 16
RSM	response surface methodology
SEM-EDX	scanning electron microscopy with energy dispersive X-ray
TCOD	total chemical oxygen demand
TEM	transmission electron microscopy
TGA	thermogravimetric analyse
WSAC	walnut shell activated carbon
XRD	X-ray diffraction

LIST OF APPENDICES

Appendix A: Standard Calibration Curve of Congo Red	93
---	----

CHAPTER 1

INTRODUCTION

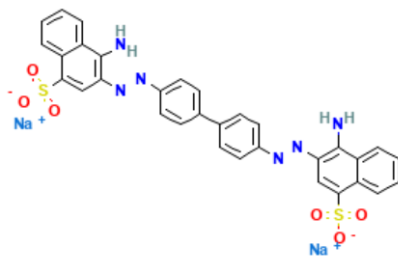
1.1 General Introduction

Rapid industrialization has negatively contributed to the environment due to the heavy discharge of pollutants into the environment by various industries. For instance, textile, leather, pharmaceuticals, foods, cosmetic, paper, and pulp industries (San, Spoann and Schmidt, 2018). Among them, the textile industry is considered one of the most significant sectors that release toxic pollutants, typically dyes, into the environment. About 5-1500 mg/L of dyes and pigments are extensively found in textile wastewater (Rafaqat et al., 2022).

Moreover, various coloured dyes and water are used during the dyeing process. As a result, they will generate a massive amount of coloured wastewater that should be treated before discharging into water bodies. Improper treatment could seriously threaten the environment and living organisms directly or indirectly (Varjani et al., 2020). It is because little concentration of synthetic dyes of less than 1 part per million (ppm) is extremely visible in the water. It affects the aesthetic value and clarity of water bodies, making it easy to identify pollution. Besides, dyes adsorb and reflect the sunlight that penetrates the water, preventing photosynthesis and the growth of aquatic creatures (Natarajan, Bajaj and Tayade, 2018). Moreover, most textile dyes are carcinogenic, mutagenic, and allergic due to their nature (Chandanshive et al., 2020).

Dyes can be classified based on their chemical structures or applications. Examples of application classification include azo, reactive, vat, sulfur, disperse, direct, acid, and basic dyes (Sid and El-Hawary, 2019). The textile dyeing process uses approximately 80 % of azo dyes (Sarkar et al., 2017). One commonly used azo dye is Congo Red (CR). The properties of CR are presented in Table 1.1.

Table 1.1: Properties of Congo Red Dye (PubChem, 2023).

Type of Dye	Azo Class
Molecular Formula	$C_{32}H_{22}N_6Na_2O_6S_2$
Chemical Structure	
Molecular Weight	696.7 g/mol
Maximum Wavelength Absorption	497 nm (Das et al., 2016)

CR brings detrimental effects to the aquatic biota. It is evident in a study where CR reduces the microalgal (*P. subcapitata*) population growth and causes sub-inhibitory effects at a low concentration of 0.04 mg/L. It also negatively impacts the microalgae's photosynthetic pigment concentration and protein content. The embryos of zebrafish are hindered from hatching, causing yolk sac edema and reduced heart beating (Hernández-Zamora and Martínez-Jerónimo, 2019). CR can be degraded into benzidine, which is carcinogenic and mutagenic to the human urinary bladder and may cause tumors in humans and animals. Besides, it may cause an allergic reaction (Gičević, Hindija and Karačić, 2020).

Therefore, minimizing or eliminating the pollution brought by the discharge of this hazardous dye through wastewater treatment is crucial. Various treatments have been proposed in the last few decades, such as membrane separation, coagulation-flocculation, adsorption, and biodegradation. However, among these treatments, adsorption remains a practical approach to removing the dye in wastewater due to its ease of operation, flexibility, and applicability. Treatment such as membrane separation is costly because of its membrane medium and fouling issues. Coagulation treatments may induce sludge formation (Saleem et al., 2019). In adsorption treatment, an adsorbent is required to adsorb the dye from dye wastewater. Activated carbon with excellent adsorption capacity, large specific surface area, and porosity makes it one of the best adsorbents for eliminating

dye (Azari et al., 2020). It has pores with a high surface area of approximately more than $1000 \text{ m}^2/\text{g}$ (Tadda et al., 2016). However, its separation from the water bodies after adsorption poses challenges because once it is saturated, the activated carbon needs to be regenerated to maintain its effectiveness. However, improper handling or disposal of spent activated carbon can result in the release of adsorbed pollutants, which can contaminate surrounding water bodies or environment (Ma, Zhang and Wen, 2021).

Hence, to improve its efficiency, activated carbon adsorption can be physically or chemically altered to enhance pollutant removal (Lee et al., 2018). In this study, powdered activated carbon (PAC) is dip-coated onto the polyurethane foam (PUF) to improve its adsorption efficiency of CR dye from synthetic dye solution. To date, only a limited number of studies are researching the use of PAC/PUF as a potential adsorbent in removing Congo Red dye. In fact, PUF is reusable, inexpensive, has high availability, and has high porosity that could promote good adsorption capacity (Wu et al., 2014). Since both PUF and PAC are promising adsorbents, coating PUF with PAC might result in an improved adsorbent that is more effective in removing CR from water bodies.

1.2 Importance of the Study

The primary importance of this study is to discover the feasibility of using a novel adsorbent made of powdered activated carbon coated on polyurethane foam (PAC/PUF) to adsorb CR dye from an aqueous solution. This discovery is important because CR dye is a toxic pollutant that can inhibit the growth of aquatic life, leading to a reduced overall metabolic rate of aquatic life. It can also persist in the environment and contaminates the water bodies over time, leading to polluted rivers, lakes, and oceans. Besides, human body can be adversely affected when its concentration is high. Therefore, the removal of CR dye is necessary (Siddiqui et al., 2023).

Another importance is to address environmental issues such as water pollution and freshwater scarcity caused by the harmful dye. Thus, using PAC/PUF, dye pollutants could be removed from the water body, resulting in cleaner wastewater that could be recycled or discharged to the river.

1.3 Problem Statement

Based on the Malaysia Third Industrial Master Plan (IMP3), Malaysia's textile and apparel industry is projected to increase its annual growth rate at 7.8 % yearly (Farhana et al., 2022). Consequently, the total amount of scheduled waste generated by the textile industry in Malaysia has risen sharply from 463.72 MT/yr (2017) to 7249.4 MT/yr (2020) (Department of Environment Malaysia, 2020). As a result, the increase in textile wastewater has contributed to the issue of freshwater scarcity.

Furthermore, as the global demand for textile goods increases, the amount of the textile industry's output and its wastewater also rise accordingly, causing it to be one of the principal global sources of severe pollution (Sarayu and Sandhya, 2012). Typically, azo dye (CR) in water is considered carcinogenic and environmentally harmful. This pollutant persists in the environment due to its aromatic structures that resist natural degradation (Harja, Buema and Bucur, 2022). Thus, throughout the past few decades and until today, dye removal from the textile industry effluent has been a pressing concern.

In addition, various conventional dye removal methods have been researched, but the majority still have drawbacks. For instance, ion exchange, coagulation-flocculation, and oxidation may be expensive and produce a large amount of sludge. Adsorption is a better and more practical method than other conventional treatments. Even so, applying activated carbon as a common adsorbent also has limitations. It may have problems with adsorbent disposal and hard separation from the dye. After treatment, it also has trouble separating from aqueous bodies and will create secondary pollution. Even when activated carbon is subjected to filtering, it may also result in the clogging of filters (Moosavi et al., 2020).

Thus, activated carbon adsorbent must be modified by supporting it to a substrate to improve its limitations. However, the research on removing dye using PAC coated on a support made of PUF is minimal. Therefore, a novel adsorbent (PAC/PUF) is synthesized in this study to investigate its dye adsorption performance and effectiveness.

1.4 Aim and Objectives

The aim of the study is to investigate the adsorption efficiency of CR dyes on PAC coated on PUF (PAC/PUF) adsorbent. Various parameters affecting adsorption are studied, including the initial concentration of dye, contact time, and pH. Several objectives are listed below to achieve the aim.

- (i) To prepare PAC coated on PUF (PAC/PUF) as adsorbent.
- (ii) To characterize the prepared PAC/PUF using Scanning Electron Microscope with Electron Dispersive X-ray (SEM-EDX), Fourier Transform Infrared (FTIR), and X-Ray Diffraction (XRD).
- (iii) To optimize the process parameters affecting Congo Red adsorption using Response Surface Methodology (RSM).
- (iv) To study the isotherm and kinetic models of adsorbate adsorption.

1.5 Scope and Limitation of the Study

The scope of the study included synthesizing and characterizing PAC/PUF adsorbent. PAC/PUF was synthesized by dip-coating PUF into PAC solution. Then, SEM-EDX, FTIR, XRD, and zeta potential analysis were performed to characterize the synthesized PAC/PUF.

Next, the dye stock solution was prepared and diluted to different concentrations to obtain a standard calibration curve. After that, RSM was utilized to design and optimize the parameters to determine the optimum adsorption efficiency of CR onto PAC/PUF. The final concentration of CR was examined by a UV-Vis spectrophotometer at a wavelength of 497 nm. Additionally, isotherm and kinetic models of adsorbate adsorption were studied. Characterization works of adsorbent were repeated after the adsorption experiment. Finally, a comparison of PAC/PUF to PAC and PUF adsorption was conducted.

The limitation of the study includes the inefficient time to study other adsorption parameters that would affect the adsorption efficiency of CR. For instance, the temperature and the shaking speed.

1.6 Contribution of the Study

This study could contribute to the textile industries towards achieving cleaner textile wastewater by using a novel adsorbent known as PAC/PUF to adsorb CR dye from the water bodies. It could also help to reduce water pollution issues to protect the environment and biodiversity from harmful and toxic CR dye. Besides, the treated textile wastewater could be recycled or undergo further treatments to obtain freshwater as part of the solutions to the water scarcity issue.

1.7 Outline of the Report

The report contained a total of five chapters. Chapter 1 outlined the general research introduction related to the issues of the study, such as the environmental impacts caused by the release of dyes into water bodies, the properties of CR, and a short review of the conventional methods of removing dyes from wastewater. Then, literature reviews relevant to the study were written in Chapter 2. Critical research on the works of other authors was carried out to compile the necessary information required in the study area. Next, the research methodology of the experiment was described in Chapter 3. This chapter explained the methods for synthesizing and characterizing PAC/PUF. Also, the ranges and levels of independent variables used to design the experiment in RSM were described. Isotherm and kinetic models of adsorbate adsorption were included as well. In Chapter 4, all the experimental results supported with thorough discussion were presented accordingly. Lastly, Chapter 5 concluded all the outcomes of this study concerning the research objectives. It also proposed other recommendations for further work.

CHAPTER 2

LITERATURE REVIEW

2.1 Introduction of Dyes

Dyes are organic compounds that can impart colours to materials such as textiles, leathers, cosmetics, and paper because of the chromophoric groups in their molecular structures. Despite that, the ability for the colour to be fixed on the material depends on the polar auxotrophic groups. The polar auxochromes allow the dyes to be water-soluble, which binds the dyes to the polar group of the textile fibers (Kumar et al., 2021).

Some of the most commonly known dyes are Congo Red (CR), methyl red (MR), methyl orange (MO), rhodamine B (RhB), and methylene blue (MB) which emerge from various industries, including the pharmaceutical, textile, leather, and food industries (Dutta et al., 2021). These dyes are commonly classified into different classes, as listed in Table 2.1. It is reported that most dyes are utilized in various industrial applications.

Table 2.1: Range of Dyes Classes (Benkhaya, M' rabet and el Harfi, 2020).

Class	Example of Dyes	Applications
Acid	Acid Blue 349, Acid Red 337, Acid Black-234	Pharmaceutical, paper, textile, and leather industries (Wu et al., 2020)
Basic	Methylene Blue, Basic Yellow 2, Basic Red 1	Synthetic fibers, paper, and ink
Direct	Congo Red Direct Blue 86, C.I. Direct Orange 26	Fibres, cotton, paper, and leather
Reactive	C.I. Reactive Red 120, Reactive Red 6, C.I. Reactive Blue 19	Dyeing and printing cotton fibers
Sulfur	Sulfur brilliant green, 1,8-Dinitronaphthalene	Dyeing textile cellulosic materials

Table 2.1 (Continued)

Class	Example of Dyes	Applications
Azo	Methy Red, Trypan Blue, Acid Orange 20	Textile fibers
Vat	Indigo carmine, Vat Black 25, Vat Yellow 1	Cotton and wool
Disperse	Disperse Red 9, Disperse Violet 26, Disperse Brown 1	Nylon, cellulose acetate, and acrylic fibres (Hassan, Awwad and Aboterika, 2009)

Among these classes, vat, sulfur, azo, and disperse dyes are not soluble in water, making them easy to remove from wastewater. In contrast, acid, basic, direct, and reactive dyes have high water solubility, making them difficult to extract from wastewater using standard separation techniques. All these water-soluble dyes are anionic except basic dyes that are cationic (Hassan and Carr, 2018).

2.2 Sources of Dyes

Dyes can be derived from natural or synthetic sources. The natural sources of dyes generally come from plants, animals, minerals, and insects. In terms of plants, dyes can be extracted from the bark of trees, flowers, or leaves (Sayem et al., 2021). On the other hand, synthetic dyes are either man-made or produced by different organic compounds. Therefore, natural sources of dyes are considered less detrimental to the environment and humans, unlike synthetic dyes. Synthetic dyes are more hazardous and toxic to both environment and human health. When used in textile industries, it might cause skin allergy or even cancer due to its carcinogenic properties (Singh and Srivastava, 2017).

Moreover, dyes can also be primarily found in the industry. Approximately 800,000 tons of dyes are produced every year on a global industrial scale (Jamee and Siddique, 2019). 54 % of dyes within this enormous production are used in the textile industries, as illustrated in Figure 2.1. The second source of dyes comes from the dyeing industries, contributing nearly 21 % and another 10 % originates from the paper and pulp industries.

Tannery and paint industries contribute a lesser percentage of 8 %, while dye manufacturing industries contribute the least rate of 7 %. However, it is to be noted that not all the dyes are fixed on the fabrics. Some dyes that are not fixed will be stripped away together with the effluent (Katheresan, Kansedo and Lau, 2018).

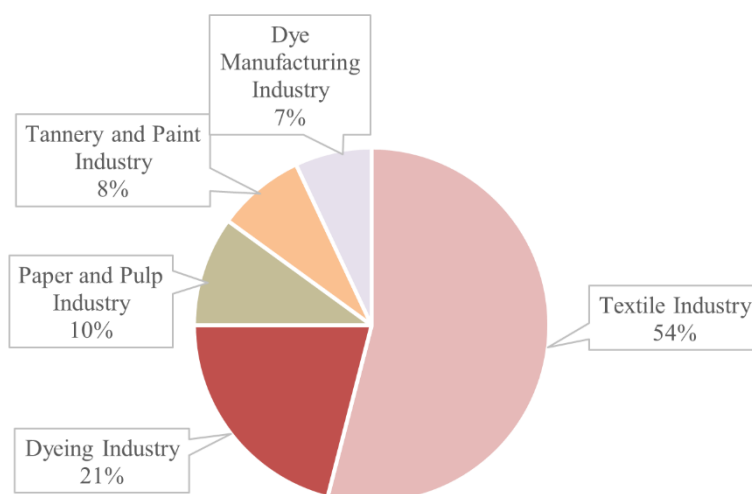


Figure 2.1: Sources of Dyes (Katheresan, Kansedo and Lau, 2018).

2.3 Environmental Impact of Dyes

The release of dyes into water bodies can result in heavily coloured wastewater. This is because the pi electrons bonded on their aromatic rings allow them to possess colours when they adsorb light in the spectrum range of 380 nm to 700 nm (Maheshwari, Agrawal and Gupta, 2021). On top of that, the presence of chromophoric groups causes them to impart colours to the water bodies, making it difficult for light to penetrate. Consequently, it will hinder the growing performance of the aquatic plants and algae inside the water. Besides, it reduces dissolved oxygen concentrations and ultimately affects marine biodiversity (Al-Tohamy et al., 2022).

Moreover, the exposure of dyes to humans or animals through oral ingestion or physical skin contact can lead to several health problems, such as skin allergies, irritations, cancers, and possible mutations. The reason is that 60-70 % of azo dyes are carcinogenic (Rawat et al., 2018). They will release aromatic amines and benzidine that are highly toxic. For instance, the

benzidine in CR dye is a bladder carcinogen which will bind to cellular macromolecules such as proteins in human organs, resulting in enzyme inhibition (Siddiqui et al., 2023). Besides, anionic dyes are more carcinogenic than cationic dyes, which can cause serious bladder cancer, asthma, and allergies. In terms of vat class dyes, they are less toxic than disperse class dyes (Maheshwari, Agrawal and Gupta, 2021).

In addition, aquatic life such as fish will be affected because when it ingests the dyes, its body systems will convert them into toxic intermediates that could harm the fish's health and predators (Elgarahy et al., 2021). Not to mention, fish suffers severe damage to kidney tissues when the dye concentrations are around 0.001-0.018 mg/L and die above 0.08 g/L (Hussain et al., 2021). For zebrafish, CR dye exposure could lead to yolk sac edema, skeletal deformities and weak heart beating rate (Hernández-Zamora and Martínez-Jerónimo, 2019). Undoubtedly, humans who consume fish as a protein source will be affected. Furthermore, the discharge of azo dyes into water bodies will contaminate the surrounding soil. The contaminated soil will reduce the productivity of any agricultural activities (Tripathi et al., 2021).

2.4 Treatment Techniques

There are various treatment techniques available to remove dyes from wastewater. These treatments can be categorized into physical, chemical, physicochemical, and biological. In terms of physical treatments, filtration, coagulation, and flocculation are some of the common dye elimination approaches used in industries (Senthil Kumar et al., 2019). In terms of chemical treatments, advanced oxidation, Fenton reaction, and photocatalytic treatments are commonly employed. Adsorption, ion exchange, and membrane treatments are popular physicochemical treatment approaches. Lastly, biological treatments include aerobic and anaerobic degradation (Katheresan, Kannedo and Lau, 2018).

However, adsorption is less expensive, most simplest, and effective treatment in removing contaminants from wastewater (Chang et al., 2018). Biological treatments may not be stable due to the culture conditions for microorganisms. For example, some microorganisms in pure culture must be cultured in highly sterile conditions, which requires high costs to do so

(Ceretta, Nercessian and Wolski, 2021). Also, biological treatment alone does not produce satisfactory removal of dyes unless combined with other treatments, such as the advanced oxidation process (AOP). For instance, the colour reduction of wastewater consisting of reactive black 5, reactive red 180, and remazol red after biological treatment was 90 % but achieved up to 100 % when biological-AOP operation was combined (Thanavel et al., 2019).

On the other hand, chemical treatments are less favoured as they are more expensive than physical or biological techniques. Chemical treatments use high electrical energy to operate. One example is the electrochemical process which requires a costly electrolytic apparatus and an increased electricity supply. Using chemicals during treatment may often result in toxic by-products that could harm the environment (Kishor et al., 2021).

Besides that, one example of physical treatment is membrane filtration. The primary drawback of the membrane filtration method is that it has a short lifespan owing to fouling, which significantly raises the expense of the procedure. Reverse osmosis, ultrafiltration, and nanofiltration are some of the common examples of membrane filtration treatments. In reverse osmosis, dye wastewater is let through a membrane with tiny pores, forcing high pressure to separate treated water from contaminants. However, dye molecules will frequently block the membrane. As a result, higher fouling will need more pressure to guarantee penetration and separation (Ezugbe and Rathilal, 2020). Table 2.2 summarizes the disadvantages of each treatment technique.

Table 2.2: Disadvantage of Conventional Treatment Technique.

Technique	Disadvantage	References
Biological	- Not stable due to different cultivation conditions - High cost - Does not produce satisfactory removal of dyes alone	(Ceretta, Nercessian and Wolski, 2021) (Thanavel et al., 2019)

Table 2.2 (Continued)

Technique	Disadvantage	References
Chemical	- More expensive than biological and physical treatment - Require high electrical energy to operate - Release toxic by-products	(Kishor et al., 2021)
Physical (membrane filtration)	- Short membrane lifespan due to fouling - High pressure and cost	(Ezugbe and Rathilal, 2020)

2.4.1 Adsorption

Adsorption is a surface process in which the adsorbate moves from a liquid or gas phase to a liquid or solid adsorbent surface and forms a thin monomolecular layer on it. The extent of adsorption is greatly influenced by the adsorbate due to its physiochemical properties (Crawford and Quinn, 2017). Some physiochemical properties include hydrophobicity, polarity, functionality, and solubility in solution (Siyal et al., 2020).

Generally, physical absorption (physisorption) and chemical adsorption (chemisorption) are the two types of adsorptions. The weak Van der Waals forces will attach the adsorbate to the adsorbent surface in physisorption. This process will not affect the chemical structure of adsorbate and adsorbent. On the other hand, chemisorption is a chemical adsorption process where the adsorbent forms covalent bonds or ionic bonds with the adsorbate. A chemisorbed species exhibits significant electrical alterations (Alaqrbeh, 2021).

The dye adsorption mechanism mainly involves electrostatic attractions, π - π interaction, and hydrogen bonding (Tran et al., 2017). Electrostatic attraction occurs when adsorbent and adsorbate (dyes) have charging states. If the adsorbent surface has a negative charging state, it will promote the adsorption of positive charging state dyes. Conversely, negative charging state dyes will be electrostatically repelled from that adsorbent (Lim et al., 2021). Meanwhile, π - π interaction occurs between the π -electrons of both carbonaceous adsorbent and the aromatic ring of the adsorbate. Strong

adsorption is observed when there is strong existence of π - π interaction (Tran et al., 2017). Lastly, hydrogen bonding forms between adsorbent and dye when the hydrogen of one element is electron deficient and interacts with another element with excess electrons. For instance, an element with an OH group interacts with O atom of another element (Ahmed et al., 2022).

2.5 Types of Adsorbents

Various adsorbents can be used to remove dyes from wastewater. For instance, activated carbon, zeolites, silica gel, and alumina. Table 2.3 shows the summary of all types of adsorbents.

2.5.1 Activated Carbon

Activated carbon is one of the well-known adsorbent materials used in the industry for various reasons. First of all, it has a high adsorption capacity to adsorb pollutants. This is attributed to its large surface area of 600 to 2000 m^2/g and various porosity textures. The microporous structures are well-characterized with an average pore diameter of 1.5 nm (Siyal et al., 2020). Besides, it can be modified relatively easily via chemical treatment to alter its chemical properties. Activated carbon can also apply in various treatment technologies, such as ultrafiltration, nanofiltration, and oxidation without generating by-products (Crini et al., 2019). Thus, activated carbon can be widely used in treating heavily contaminated effluent.

Commercial activated carbon can be prepared from coal, coconut shells, wood, etc. There is also activated carbon prepared from waste materials such as rice husk, walnut shells, orange peel, and berry leaves (Ahmad et al., 2019b). Activated carbon commonly comes in powder and granular forms, known as powdered activated carbon (PAC) and granular activated carbon (GAC), respectively.

GAC has a high adsorption capacity that could be used to treat wastewater effectively. GAC could be used to biologically treat wastewater, known as biologically active granular activated carbon (BAC). It was found that 71 % of the total chemical oxygen demand (TCOD) in the wastewater could be removed by the BAC (Sharaf and Liu, 2021). In addition, GAC is reusable and regenerable after exhaustion. It could also effectively eliminate

the majority of micro-contaminants. However, it is costly and requires regular reactivation due to the limited adsorption capacity, resulting in a higher process expense (Brandt et al., 2017).

PAC is widely used in wastewater treatment to remove micro-pollutants due to its good adsorption capacity, mesoporous and fine structure properties (Mailler et al., 2016). However, its disadvantages include challenging containment and possible dust formation due to its fine powder structure. Thus, caution must be practiced when handling PAC without creating a nuisance or causing a dust explosion (Brandt et al., 2017). Another disadvantage of PAC is that it may be difficult to separate from water bodies and generates secondary pollution (Moosavi et al., 2020).

Furthermore, many studies have been done on removing dyes from wastewater using activated carbon. For instance, methylene blue (MB) dye was successfully adsorbed by activated carbon derived from the rosemary (RM) plant, denoted as RMAC. A maximum adsorption capacity of 110.65 mg/g using 0.05 g/L of RMAC and an initial dye concentration of 300 mg/L was achieved. The adsorption efficiency achieved was more than 85 % (Amin, Alazba and Shafiq, 2017). Additionally, eosin Y and indigo carmine acid dyes were successfully adsorbed by activated carbon, whereby the adsorption efficiency of activated carbon could achieve up to 99.4 % for eosin Y removal and 92.38 % for indigo carmine. The activated carbon dosage was 1g/L and the contact time was 60 min (Alwi et al., 2020).

Moreover, PAC, the promising adsorbent, achieved 99 % CR dye removal when the PAC dosage was 0.09 g (Nizam et al., 2021). Another study also showed the removal efficiency of RhB and CR by activated carbon derived from palm tree fiber (PTFAC) increased to over 99 % when the adsorbent dose increased from 0.05 g to 0.25 g (Alhogbi et al., 2021).

2.5.2 Zeolites

Zeolite is a substance that has high adsorption capacity, excellent selectivity, is easy to regenerate and does not quickly get saturated, which makes it a popular adsorbent (Laksmono et al., 2018). It is a porous aluminosilicate that has a three-dimension (3D) structure. Its main building blocks are tetrahedra of SiO_4 , AlO_4 , and an oxygen atom joining these two units (Ramezani, Azizi and

Hosseini, 2017). It is highly negative-charged due to the presence of aluminium (Al). By controlling the ratio of SiO_4 and AlO_4 , the adsorption properties can be adjusted.

The application of zeolites in the adsorption of dyes is reported in many research. For instance, magnetic zeolite-hydroxyapatite nanocomposites were used to remove congo red (CR), reactive orange 5 (RO5), and RO16 from the waste solution. 104.05 mg/g (CR), 92.45 mg/g (RO5), and 88.31 mg/g (RO16) adsorption capacities were obtained at an equilibrium time of 30 min and an initial dye concentration of 80 ppm. The adsorbent dosage to achieve maximum adsorption capacity was fixed at 0.005 g (Piri et al., 2019). Besides, 4A zeolite adsorbent was used to remove MB and malachite green (MG) dyes from the waste solution. It was found that the adsorption capacities of 9.95 mg/g of MB and 45.64 mg/g of MG were achieved at an adsorbent dosage of 0.1 g (Imessaoudene et al., 2022).

2.5.3 Silica Gel

Silica gel having mesoporous properties is mainly made of SiO_2 . It is utilized as an adsorbent for treating wastewater because of its durability, broad pore channels, the potential for reuse, reduced cost, high surface area, excellent chemical stability, and strong mechanical resistance (Patra et al., 2017). However, its disadvantage is that it is less adsorptive than zeolites when the moisture level is low (Pourhakkak et al., 2021).

A study used graphene oxide/silica as the adsorbent to adsorb CR from an aqueous solution. It was found that 98 % removal of CR was achieved when 0.005 g of graphene oxide/silica was used. The removal rate reached equilibrium at an adsorbent dosage of 0.01 g (Zhang et al., 2020). Besides, cationic-modified silica gel was investigated by Zhang et al. (2019) to remove reactive black 5 and reactive red 239 from wastewater. It achieved a maximum adsorption capacity of 190.0 mg/g and 178.2 mg/g for reactive black 5 and reactive red 239, respectively. Besides, silica gel supported on a dinitro calix-4-arene cage (DNCC) was studied to carry out the adsorption of MB. The adsorbent achieved an adsorption capacity of 212.77 mg/g at 0.02 g of adsorbent dosage and pH 12 (Temel, Turkyilmaz and Kucukcongar, 2020).

2.5.4 Alumina

Alumina is known to have a large surface area, strong mechanical properties, and good heat resistivity (Terrazas et al., 2021). It is also environmentally stable due to the presence of Lewis acid sites (Asim et al., 2019). Thus, alumina has been researched as a feasible adsorbent for removing dyes from wastewater.

A study used gamma alumina adsorbent synthesized from aluminium residue to remove basic fuchsin (BF), MB, and crystal violet (CV) dye from water bodies. The synthesized adsorbent was highly mesoporous with a high surface area of 304.31 m²/g. Due to these properties, a maximum adsorption capacity of 57.81 mg/g, 31.92 mg/g, and 32.92 mg/g was achieved for MB, CV, and BF, respectively at an initial concentration of dye of 100 mg/L. It was said that alkali pH 9 was the best condition, while alleviated adsorbent dosage will not further increase the removal of dyes due to decreased number of active sites. Besides, the equilibrium time needed for maximum adsorption of CV was within 30 min (Fernandes et al., 2021).

Table 2.3: Summary of Various Adsorbents.

Adsorbent	Advantage	Disadvantage	Important Findings	Reference
Activated Carbon	<ul style="list-style-type: none"> - High adsorption capacity - Large surface area - Various porosity - Easily modified chemically - Applied in various treatment technologies - Treat heavily contaminated effluent 	<ul style="list-style-type: none"> - GAC is costly and requires regular reactivation - PAC is difficult to contain and possible dust formation - Difficult to separate from water bodies - Generates secondary pollution 	<ul style="list-style-type: none"> - 110.65 mg/g adsorption capacity for MB dye using RMAC adsorbent dosage of 0.05 g/L. - 99.4 % adsorption efficiency in removing eosin Y and 92.38 % for indigo carmine using 1g/L of adsorbent. - 99 % CR dye removal using PAC dosage of 0.09 g. - 99 % removal efficiency of RhB and CR by PTFAC using an adsorbent dose of 0.25 g to 0.05 g. The equilibrium is reached when PTFAC is at 0.1 g. 	<ul style="list-style-type: none"> (Siyal et al., 2020) (Crini et al., 2019) (Brandt et al., 2017) (Moosavi et al., 2020) (Amin, Alazba and Shafiq, 2017) (Alwi et al., 2020) (Nizam et al., 2021) (Alhogbi et al., 2021)

Table 2.3 (Continued)

Adsorbent	Advantage	Disadvantage	Important Findings	Reference
Zeolites	<ul style="list-style-type: none"> - High adsorption capacity - Great selectivity - Easy to regenerate - Not quickly get saturated 	-	<ul style="list-style-type: none"> - 104.05 mg/g (CR), 92.45 mg/g (RO5), and 88.31 mg/g (RO16) adsorption capacity are achieved using an adsorbent dosage of 0.005 g. - Adsorption capacities of 9.95 mg/g for MB and 45.64 mg/g for MG are achieved at an adsorbent dosage of 0.1 g 	<ul style="list-style-type: none"> (Laksmono et al., 2018) (Piri et al., 2019) (Imessaoudene et al., 2022)
Silica Gel	<ul style="list-style-type: none"> - Mesoporous properties - Durable - Broad pore channels - Potential for reuse - Reduced cost - High surface area - Great chemical stability - Strong mechanical resistance 	- Less adsorptive than zeolites when the moisture level is low	<ul style="list-style-type: none"> - 98 % removal of CR is achieved when 0.005 g of graphene oxide/silica is used. - Adsorption capacity of 190.0 mg/g and 178.2 mg/g for reactive black 5 and reactive red 239, respectively. - 212.77 mg/g adsorption capacity for MB is achieved using 0.02 dosage of silica gel supported dinitro calix[4]arene cage. 	<ul style="list-style-type: none"> (Patra et al., 2017) (Pourhakkak et al., 2021) (Zhang et al., 2020) (Zhang et al., 2019) (Temel, Turkyilmaz and Kucukcongar, 2020)

Table 2.3 (Continued)

Adsorbent	Advantage	Disadvantage	Important Findings	Reference
Alumina	<ul style="list-style-type: none"> - Large surface area - Strong mechanical properties - Good heat resistivity - Environmentally stable 	-	<ul style="list-style-type: none"> - Adsorption capacity of 57.81, 31.92, and 32.92 mg/g could be achieved for MB, CV, and BF, respectively 	<ul style="list-style-type: none"> (Terrazas et al., 2021) (Asim et al., 2019) (Fernandes et al., 2021)

2.6 Polyurethane Foam

Using raw adsorbents alone may not effectively remove pollutants in water and wastewater. Therefore, raw adsorbents are frequently modified to improve their removal efficiencies. Adding support is one of the methods to modify the raw adsorbents (Singh, Wasewar and Kansal, 2020).

Polyurethane foam (PUF) is an example of adsorbent support. It is widely used in the construction and automotive industry (Francés and Bañón, 2014). However, PUF has recently expanded its application to wastewater treatment. It has begun to use as a support for adsorbents and catalysts due to its open porous structure that offers a large surface area to recover sorbent and catalyst easily for water treatment (Ahmad et al., 2019a).

The roughness, porosity, pore size, and specific area of PUF will affect its adsorption efficiency. Regarding roughness, the liquid penetration rate into the porous medium with a rough surface is nearly two times higher than porous materials with smooth surfaces. Low roughness indicates higher hydrophobic properties, which result in decreased water adsorption. A study on the adsorption of biomass found that the high porosity and small pore size of PUF enabled the biomass to be removed at an efficiency of 62.2 % (Dacewicz and Grzybowska-Pietras, 2021). A similar observation was reported by Machdar et al. (2018), whereby the use of a small pore size of PUF, about 0.56 mm, in a down-flow hanging sponge (DHS) reactor could remove organic pollutants, decreasing soluble COD to 65 % and total COD to approximately 76 % from domestic wastewater.

Besides, its high surface area could facilitate different adsorbents, typically activated carbon. It is because activated carbon in the form of granular or powdered is challenging to handle and must be immobilized to improve its adsorption practicality. This was proven in a study by Keshavarz et al. (2016), whereby impregnating PUF with activated carbon increased the oil adsorption capacity by 33.2 % compared to using PUF only. It was because adding activated carbon to PUF enhanced the surface roughness, making it more easily to hold the oil.

2.7 Synthesis of Adsorbent

There are a few methods to produce PAC/PUF adsorbent. Each method differs in its complexity.

2.7.1 Dip-Coating

Dip-coating is a simple method to produce PUF-related adsorbents. It mainly involves stirring, sonicating, and drying. A few studies have been utilizing this method to make adsorbents. For instance, PUF was dip-coated with compact disc-derived activated carbon to obtain AC/PUF adsorbent. PUF was first cleaned with acetone in an ultrasonic bath for 15 min. Then, activated carbon was added to the ethanol solution and sonicated for 15 min to obtain the AC solution. The PUF was then dried and dipped into the AC solution under slow stirring for 15 min. Finally, the synthesized AC/PUF was dried at 60-70 °C (Mallakpour and Behranvand, 2020). Furthermore, Singh, Sharma and Vaish (2019) used the dip-coating method to synthesize diesel exhaust emission soot (DEES) on PUF. Firstly, 100 mg of DEES was added to an ethanol solution (100 mL) and sonicated for 30 min. Then, PUF was washed in acetone solution and dried in an oven for 1 hr. After that, the PUF was dip-coated in DEES solution for 20 min. The final DEES-PUF was dried in an oven at 80 °C.

2.7.2 Impregnation

This method involves precursor solution preparation, crosslinking, carbonization, and activation. According to Udayakumar et al. (2021b), impregnation was done by mixing 40 mL of 2.8 wt% dilute sulphuric acid with 100 g concentrated sucrose in a beaker. Then, the mixture was heated at 80 °C under continuous stirring to obtain acidified sucrose solution. PUF cubes were immersed into the acidified sucrose solution for 12 h for impregnation. After impregnation, PUF cubes were dried overnight at room temperature and placed in an oven for 10 h at 110 °C to crosslink. The resultant PUF sample was carbonized at 700 °C or 900 °C in a tube furnace filled with nitrogen for 1 h. A heating rate of 10 °C/min was supplied. Finally, the sample was activated inside a tube furnace under a CO₂ flow of 200 mL/min at 90 °C or 1000 °C. The heating rate was 10 °C/min for 100 min. An alternative method was to

activate PUF immediately in the CO₂ atmosphere without carbonization (Udayakumar et al., 2021a).

2.8 Composite Adsorbents Applications

Nowadays, adsorbents with supporting substrates, also known as composite adsorbents, have become more commonly used due to their numerous applications in wastewater treatments. They have enhanced physical and chemical properties that can improve the adsorption performance (Adeleke et al., 2019).

According to Quesada et al. (2022), activated carbon on chitosan hydrogel substrate was used to remove caffeine from tap water and synthetic hospital wastewater. It was found that chitosan hydrogel had a low specific surface area, thus showing no adsorption capacity. However, adding activated carbon on chitosan hydrogel enhanced the adsorption capacity to 121.90 mg/g. Besides, activated carbon on polyurethane foam effectively improved the adsorption efficiency of metals from an aqueous solution. Lead and copper ions were adsorbed onto the composite, achieving 77 % lead and 40 % removal of copper ions (El Malti et al., 2021).

Furthermore, activated carbon with MnFe₂O₄ composite could adsorb methyl red dye at a maximum adsorption capacity of 81.97 mg/g even though the surface area was smaller than activated carbon alone (Riyanti et al., 2018). In addition, applying activated carbon on NiFe₂O₄ could effectively adsorb ibuprofen and ketoprofen from pharmaceutical wastewater. This composite could be easily separated after adsorption because of its magnetic properties (Fröhlich, Foletto and Dotto, 2019).

2.9 Factors Affecting Adsorption Efficiency

Various factors affect the adsorption efficiency of CR onto PAC/PUF. These factors include the initial concentration of dye, pH, and contact time.

2.9.1 Initial Concentration of Dye

The initial concentration of dye will have an impact on the adsorption capacity of the adsorbent. The adsorption capacity is expected to increase as the initial concentration of dye increases. It was evident in a study where the adsorption of methylene blue (MB) by grass-derived activated carbon (GWAC) increased from 66.8 mg/g to 372.2 mg/g when the initial concentration of MB increased from 50 mg/L to 300 mg/L. The other experimental parameters were kept constant. For example, the solution pH was 10 and the dosage of GWAC at 0.06 g/100 mL. This observation may be due to the formation of MB concentration gradient which could improve the MB diffusion into the GWAC pore sites. These pore sites provided the active sites for adsorption to occur. Thus, more dyes were transported to the active sites of GWAC to carry out adsorption (Abdulhameed et al., 2021).

Another similar finding also reported the adsorption capacity of modified activated carbon to adsorb MB increased from 64.4 mg/g to 195.8 mg/g when the initial concentration of MB increased from 10 mg/L to 50 mg/L. However, once the equilibrium was reached, any further addition of MB concentration will not increase the adsorption amount since all the adsorbent active sites were adsorbed (Kuang, Zhang and Zhou, 2020). Besides that, Rhodamine B (RhB) adsorption by PUF-derived activated carbon composites also showed a similar trend (Shivaprasad et al., 2019).

Moreover, the removal efficiency of the CR using mesoporous activated carbon achieved 94.72 % when the initial dye concentration rose from 50 mg/L to 200 mg/L (Ma et al., 2020). This observation was further proven by Lafi, Montasser and Hafiane (2019) and Patra et al. (2020). Table 2.4 shows the typical range of initial concentration of adsorbate studied by other authors.

Table 2.4: Range of Initial Concentration of Dye Reported by Other Studies.

Range of Initial Concentration of Dye	Fixed Parameters	Adsorbate	Adsorption Capacity/ Efficiency	References
50 – 300 mg/L	pH: 10 Adsorbent dosage: 0.06 g/100 mL	MB	364.2 mg/g	(Abdulhameed et al., 2021)
10 – 50 mg/L	pH: 5 Adsorbent dosage: 15 mg/ 100 mL	MB	96.6 % removal efficiency	(Kuang, Zhang and Zhou, 2020)
25 – 100 mg/L	pH: 8 Adsorbent dosage: 1.5 g/ 150 mL	RhB	17.99 mg/g	(Shivaprasad et al., 2019)
50 – 200 mg/L	pH: 7 Adsorbent dosage: 0.8 g/L	CR	94.72 % removal efficiency	(Ma et al., 2020)
20 – 120 mg/L	pH: 3 Adsorbent dosage: 0.1 g/ 25 mL	CR	51.87 mg/g	(Lafi, Montasser and Hafiane, 2019)
50 – 250 mg/L	pH: 2 Adsorbent dosage: 0.005 g/ 25 mL	CR	~85 %	(Patra et al., 2020)

2.9.2 pH

Another factor that affects the adsorption efficiency is the solution pH. The effect of solution pH on the adsorption efficiency differs for anionic and cationic dyes. According to Abate et al. (2020), the adsorption efficiency of cationic malachite green (MG) dye by activated carbon increased with increasing solution pH (2-11) until equilibrium was attained. This observation may be attributed to the formation of negative charges on the adsorbent surface when the pH increased. As a result, the positively charged MG and the negatively charged adsorbent experienced a strong electrostatic attraction. If the solution pH decreases, the adsorbent surface and MG dye will be protonated, resulting in repulsion and decreased removal efficiency. In addition, Jawad and Abdulhameed (2020) research also showed similar observations. It stated that when the pH of the solution increased from 3 to 10, the amount of MB removed was increased. Other experimental parameters were kept constant such as the temperature at 40 °C and the adsorbent dose at 0.06 g.

However, this result trend is contrary in removing anionic dyes. The removal efficiency of anionic dyes is expected to decrease when the pH increases. For instance, removing tartrazine and sunset yellow dyes by biowaste-derived activated carbon decreased with increasing solution pH. The reason was that the active adsorbent sites became more and more negatively charged when the pH increased. Since the tartrazine and sunset yellow dyes were negatively charged, the dyes repelled the adsorbent, resulting in less electrostatic attraction (Chukwuemeka-Okorie et al., 2021). In addition, biomass-based activated carbon achieved nearly 100 % adsorption efficiency of CR when the pH was low (Nizam et al., 2021). This observation was also proven by other studies from Masoudian, Rajabi and Ghaedi (2019) and Mandal et al. (2021). Table 2.5 shows the typical range of pH studied by other authors.

Table 2.5: Range of pH Reported by Other Studies.

Range of pH	Fixed parameters	Adsorbate	Adsorption Capacity/ Efficiency	Reference
2 – 12	Initial concentration of dye: 10 mg/L Adsorbent dosage: 0.5 g / 50 mL	MG	98.8 %	(Abate et al., 2020)
3 – 10	Adsorbent dosage: 0.1 g / 100 mL	MB	96.7	(Jawad and Abdulhameed, 2020)
1 – 10	Initial concentration of dye: 150 mg/L Adsorbent dosage: 0.1 g	Tartrazine and sunset yellow dye	~30 mg/g (tartrazine) ~ 22 mg/g (sunset yellow)	(Chukwuemeka-Okorie et al., 2021)
2 – 10	Initial concentration of dye: ~ 70 mg/L Adsorbent dosage: 0.01 g	CR	~100 %	(Nizam et al., 2021)
2 – 9	Initial concentration of dye: 14.7 mg/L Adsorbent dosage: 0.04 g/ 50 mL	CR	~80 %	(Masoudian, Rajabi and Ghaedi, 2019)
3 – 8	Initial concentration of dye: 20 mg/L Adsorbent dosage: 0.05 g/ 40 mL	CR	78.9 %	(Mandal et al., 2021)

2.9.3 Contact Time

Adsorption of dyes is a time-dependent process. The higher the contact time between the dyes and the adsorbent, the higher the adsorption capacity of the adsorbent. For instance, the adsorption of CR using low-cost *Typha australis* leaves adsorbent increased with time (0 – 90 min) until equilibrium was reached at 60 to 70 min (Ali et al., 2021). It was because many active sites were available on the adsorbent surface for rapid adsorption in the initial stage. However, the saturation of CR molecules increased with increased contact time, which hindered the binding sites of adsorbed molecules. As a result, the adsorption amount gradually became constant. Besides, according to Wang, Ma and Sun (2022), removing MB dye using activated carbon achieved a maximum adsorption capacity of 15 mg/g and an adsorption efficiency of 90 % when the contact time increased to 8 h. Other experimental parameters were kept constant such as the initial MB concentration. During the first 2 h, the adsorption rate was very fast until it reached equilibrium at 8 h. After that, prolonging contact time will not increase the adsorption capacity but resulted in a constant value.

Another study using magnetic palm shell-activated carbon achieved an adsorption capacity of 9.18 mg/g of CR when the pH was 6 and the initial concentration of dye was 0.03 g/ 30 mL (Kittappa et al., 2020). This observation was proven by other studies from Latinwo et al. (2019) and Mandal et al. (2021). Table 2.6 shows the typical range of contact time used for the adsorption of dyes.

Table 2.6: Range of Contact Time Reported by Other Studies.

Range	Fixed Parameters	Adsorbate	Adsorption Capacity/ Efficiency	Reference
0 – 90 min	pH: 2 Initial concentration of dye: 30 mg/L	CR	2.403 mg/g	(Ali et al., 2021)
2 – 1440 min	pH: 6 Initial concentration of dye: 10 mg/L	MB	15 mg/g / 90 %	(Wang, Ma and Sun, 2022)
60 – 200 min	pH: 6 Initial concentration of dye: 0.03 g/ 30 mL	CR	9.18 mg/g	(Kittappa et al., 2020)
30 – 240 min	Adsorbent dosage: 10 g/ 100 mL Initial concentration of dye: 500 mg/L	CR	77.49 %	(Latinwo et al., 2019)
20 – 120 min	pH: 4 Adsorbent dosage: 0.05 g/ 40 mL Initial concentration of dye: 20 mg/L	CR	78.9 %	(Mandal et al., 2021)

2.10 Design of Experiment

Design of experiment (DOE) is a structured approach used for planning experiments and analyzing combinations of input variables, resulting in an output variable with the optimized values. Design Expert is one of the well-known analytical and graphical tools to perform experiment design. A response surface methodology (RSM) can be used to create a design space with the input variables and estimate the value of responses of every possible combination of the variables. In RSM, response surfaces are graphical representations that describe the interaction between process variables and how they affect the response. On the other hand, the polynomial quadratic model represents the relationship between the response and the variables as shown in Equation 2.1 (Kumari and Gupta, 2019).

$$Y = \beta_o + \sum_{i=1}^n \beta_i X_i + \sum_{j=1}^n \beta_{ii} X_i^2 + \sum_{i=1}^{n-1} \sum_{j=i+1}^n \beta_{ij} X_i X_j + E \quad (2.1)$$

Where;

Y = Predicted response

β_o = Regression Coefficient

$\beta_i, \beta_{ii}, \beta_{ij}$ = Linear, quadratic and interaction coefficients, respectively

X_i and X_j = Coded values of process variables

E = Experimental error

Multiple designs in the RSM can be chosen such as the Box-Behnken design, one-factor design, and central composite design (CCD). CCD is widely used by other authors to access the quadratic response surface. Generally, CCD consists of $2n$ factorial runs, $2n$ axial runs, and n_c for centre runs (n_c). The factorial points are coded with a value of ± 1 , while the axial points are coded with a value of $\pm \alpha$. Centre points are coded with 0. The value of the α is determined based on the calculation possibilities and the required precision to estimate the surface response. The total number of runs (N) to conduct will depend on $N = 2^n + 2n + n_c$. Thus, the number of runs for the complete design will increase with the number of variables (n) (Behera et al., 2018).

In CCD-based RSM, the significance of the regression model and the independent variables can be examined using analysis of variance (ANOVA). For instance, the F-value compares the model importance with the residual error, and the P-value gives the probability of the F-value to test the null hypothesis. If the P-value is less than 0.05 and the F-value is high, the model terms are significant. On top of that, ANOVA provides information on the model's coefficient of determination (R^2) value. If the R^2 value is greater than 0.9, it implies that the model is effective in estimating the experimental variables. Besides, ANOVA provides 2D contour plot or 3D surface of the response surface to analyze the interaction between process variables. Examples of 2D and 3D surface plots obtained by a study on the adsorption of CR using exfoliated graphite are illustrated in Figure 2.2 (Van Pham et al., 2019). Lastly, the validation of the model can be determined by conducting experiments based on the given optimum operating conditions generated by RSM.

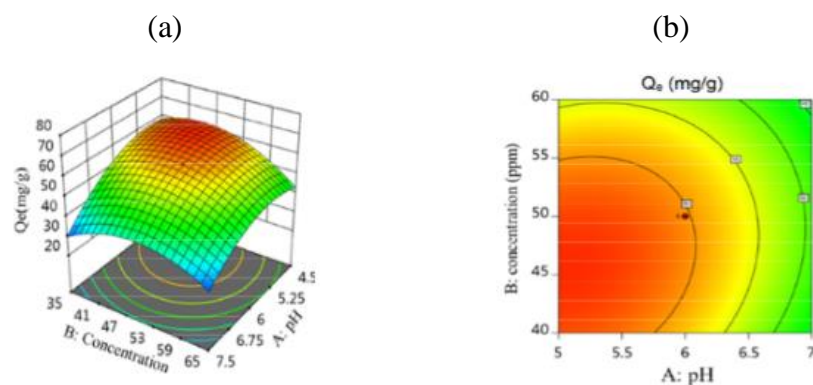


Figure 2.2: Response Plots of Adsorption of Congo Red (a) 3D Surface Response Plots and (b) 2D Contour Plots (Van Pham et al., 2019).

2.11 Characterization of PAC/PUF

Characterization of PAC/PUF is essential to understand its physical and chemical properties before and after the adsorption experiment. The characterization methods include scanning electron microscopy with energy dispersive X-ray (SEM-EDX), Fourier-Transform infrared spectroscopy (FTIR), and X-ray diffraction (XRD).

2.11.1 Scanning Electron Microscopy with Energy Dispersive X-Ray (SEM-EDX)

SEM analysis is used to investigate the morphological and surface changes of PAC/PUF by scanning the adsorbent sample using highly concentrated electron beams. These electron beams are known as the primary electrons. The outgoing electrons from each part of the sample, known as the secondary electrons, will be collected to produce an image. The image provides information such as topography, morphology, composition, etc. Thus, properties of PAC/PUF, such as texture, size, and shape can be analyzed. The operation is done under a vacuum condition to prevent unwanted interactions between electrons and the atmosphere (Akhtar et al., 2018). Figure 2.3 shows the sample SEM images of AC/PUF analyzed by a study on the adsorption of MB from wastewater.

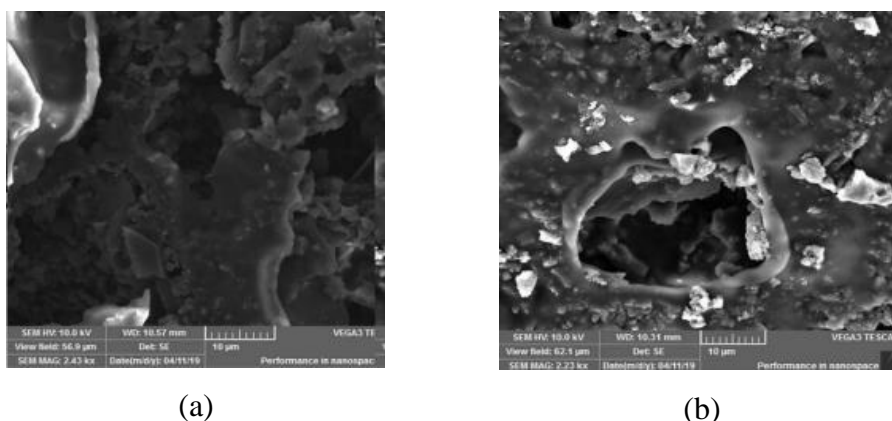
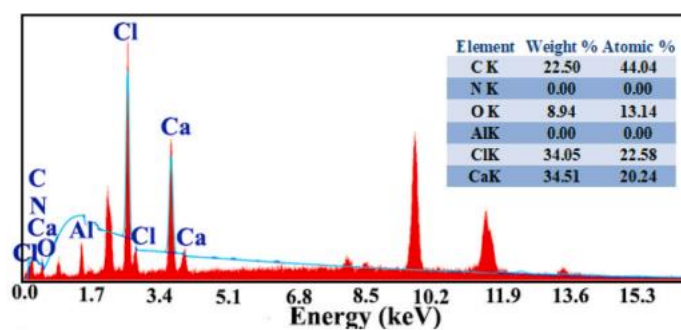
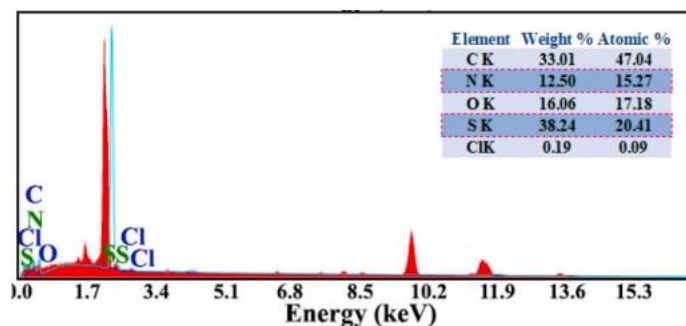


Figure 2.3: SEM Images of AC/PUF (a) Before Adsorption and (b) After Adsorption Experiment (Wu et al., 2019).

EDX analysis allows the determination of elements present in the PAC/PUF. It will generate characteristic X-rays in atoms due to the incident electron beams on the sample. Through the energy of the X-rays, a spectrum is produced which allows observation of the elemental information. Therefore, SEM with EDX characterization allows the information on both surface morphology and elemental composition of PAC/PUF to be obtained. Examples of the EDX spectrum for the MB adsorption by disc-derived activated carbon on polyurethane foam (DAC/PUF) is presented in Figure 2.4.



(a)



(b)

Figure 2.4: EDX Spectrum of DAC/PUF (a) Before Adsorption and (b) After Adsorption Experiment (Mallakpour and Behranvand, 2021).

2.11.2 X-Ray Diffraction (XRD)

The crystallinity of the PAC/PUF sample can be analyzed using XRD characterization. It works by shooting a beam of X-rays through the sample, and the scattering or diffraction of the X-rays will be collected (Raval et al., 2019). XRD satisfies Bragg's Law and the diffractions are detected by scanning the sample using a range of 2θ angles. Equation 2.2 shows the Bragg's Law (Dutrow and Clark, 2019).

$$\eta\lambda = 2d\sin\theta \quad (2.2)$$

Where,

η = order of reflection

λ = wavelength of X-ray, m

d = distance between two lattice planes, m

θ = angle between incident X-ray and normal to the reflecting plane

2.11.3 Fourier-Transform Infrared (FTIR) Spectroscopy

The functional groups of PAC/PUF adsorbent can be determined using FTIR spectroscopy by reading the FTIR spectra generated. A beam of infrared (IR) irradiation will be generated from a source and passes through an interferometer. The interferogram, which results from constructive and destructive interference caused by the different path lengths of the beam, will be produced. A detector is used to measure the energy against time. In the end, a spectrum is generated (Mohamed et al., 2017).

A sample FTIR spectrum of CR and MB adsorption by walnut shell activated carbon (WSAC) is shown in Figure 2.5. It could be observed that the FTIR spectra of WSAC before and after adsorption were similar, with prominent bands around 3400 cm^{-1} , 1610 cm^{-1} , and 1110 cm^{-1} , representing O-H, C=C and C-C-C bonds respectively (Li et al., 2020). Figure 2.6 shows the spectrum of PUF modified with recycle PUF polyol (Kraitape and Thongpin, 2016). Different wavenumbers translate different functional groups. Table 2.7 shows the typical wavenumber of various functional groups.

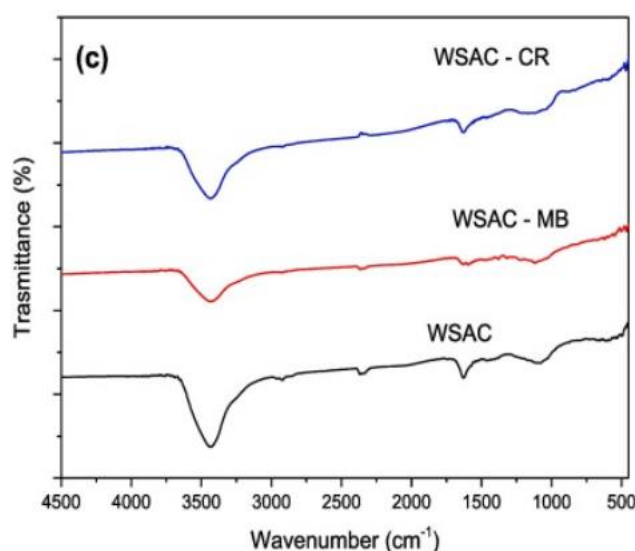


Figure 2.5: FTIR Spectrum of Congo Red and Methylene Blue Adsorptions by Walnut Shell Activated Carbon (Li et al., 2020).

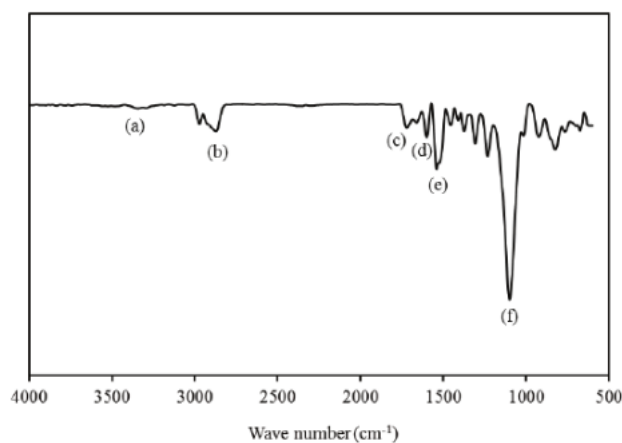


Figure 2. FTIR spectra of PU foam modified with recycle PU foam polyol

Figure 2.6: FTIR Spectrum of PUF Modified with Recycle PUF Polyol (Kraitape and Thongpin, 2016).

Table 2.7: Typical Wavenumber for Different Functional Groups (Mohamed et al., 2017).

Functional Group	Type	Wavenumber (cm ⁻¹)
C–H	Alkanes	3000 – 2850
C=C	Alkenes/Aromatic	1475 – 1680
O–H	Alcohol	3400 – 3650
C≡O	Alkyne	2250 – 2100
C=O	Aldehyde	1740 – 1720
	Ketone	1725 – 1705
	Carboxylic Acid	1725 – 1705
	Ester	1750 – 1730
C≡N	Nitriles	2260 – 2240
N–H	Amines	3500 – 3100

2.12 Adsorption Model

Two major adsorption models are used to explain the adsorption process: isotherm and kinetic. The physical, chemical, and mathematical analysis of the adsorption isotherm model can be used to infer quantitative information about the relationship between the adsorbent and the adsorbate, the affinity of the adsorbents at equilibrium, surface characteristics, and the adsorption mechanism. Using the equilibrium data obtained from the experiment, the

modelling of an adsorption system in a real treatment plan becomes feasible (Sohbatzadeh et al., 2016). Two main adsorption isotherm models used are Langmuir and Freundlich models.

On the other hand, kinetic analysis is necessary to understand the adsorption mechanism better. Therefore, kinetic models are developed to analyze the changes in adsorbent concentration with time. Pseudo first-order (PFO) and Pseudo second-order (PSO) are generally used as kinetic models in adsorption studies (Revellame et al., 2020).

2.12.1 Langmuir Isotherm Model

A few assumptions are applied in the Langmuir adsorption model. Firstly, the surface of an adsorbent is homogeneous, resulting in equivalent sites. Secondly, a single layer of adsorbed molecules is formed on the adsorbent surface. Thirdly, no lateral interactive effects between adjacent adsorbed molecules is assumed. Lastly, each specific active site will adsorb only one adsorbate molecule (Sahoo and Prelot, 2020).

The equation of Langmuir isotherm is expressed in Equation 2.3. The linearization form of the Langmuir isotherm is illustrated in Equation 2.4.

$$q_e = \frac{q_0 K_L C_e}{1 + K_L C_e} \quad (2.3)$$

Where;

q_e = Amount adsorbed at equilibrium (mg/g)

q_0 = Amount of dye adsorbed (mg/g)

K_L = Langmuir constant (L/mg)

C_e = Adsorbate concentration at equilibrium (mg/L)

$$\frac{C_e}{q_e} = \frac{1}{K_L q_0} + \frac{C_e}{q_0} \quad (2.4)$$

Based on the Langmuir equation in linear form, $\frac{C_e}{q_e}$ against C_e is plotted to obtain a straight-line graph. The slope of the graph determines the $\frac{1}{q_0}$ and the intercept is represented by $\frac{1}{K_L q_0}$.

The separation factor is another critical parameter used to explain the favourability of adsorption. The separation factor can be defined in Equation 2.5. Four possible outcomes of the separation factor can be obtained: (i) favourable ($0 < R_L < 1$), (ii) unfavourable ($R_L > 1$), (iii) irreversible ($R_L = 0$), or (iv) linear ($R_L = 1$) (Ajenifuja, Ajao and Ajayi, 2017).

$$R_L = \frac{1}{1+K_L C_0} \quad (2.5)$$

Where;

R_L = Separation factor

K_L = Langmuir constant, L/mg

C_0 = Adsorbate molecules at initial concentration, mg/L

2.12.2 Freundlich Isotherm Model

Freundlich initially introduced Freundlich isotherm as an empirical equation in 1906. Since then, the Freundlich isotherm has been applicable in describing multilayer adsorption and equilibrium adsorption on heterogeneous surfaces of adsorbents (Liu et al., 2019). The non-linear Freundlich equation is expressed using Equation 2.6, while the linearised form is described using Equation 2.7 (Wang and Guo, 2020).

$$q_e = b C_e^{\frac{1}{n}} \quad (2.6)$$

$$\ln q_e = \ln b + \frac{1}{n} \ln C_e \quad (2.7)$$

Where;

q_e = Amount adsorbed at equilibrium, mg/g

b = Adsorption capacity, L/mg

C_e = Adsorbate concentration at equilibrium, mg/L

$\frac{1}{n}$ = Adsorption intensity or surface heterogeneity

The higher the value of $\frac{1}{n}$ indicates that the system is likely to have stronger adsorption forces. It also suggests the favourability of adsorbate on the adsorbent surface when n values range from 1-10. Besides, the value of this fraction also provides information about the system's capacity (Liu et al., 2019).

2.12.3 Pseudo First-Order Kinetic Model

Lagergren first developed the PFO equation in 1898. It describes the adsorption of solute onto adsorbent based on first-order reaction rate. The differential form of the PFO equation can be expressed using Equation 2.8, whereas the linear form can be illustrated using Equation 2.9. However, linearization may increase the error level. Different adsorption conditions such as high adsorbent dosage will affect the PFO kinetic model applicability (Kajjumba et al., 2018).

$$\frac{dq_t}{dt} = k_1(q_e - q_t) \quad (2.8)$$

$$\ln(q_e - q_t) = \ln q_e - k_1 t \quad (2.9)$$

Where;

q_t = Amount of dye on PAC/PUF at time t , mg/g

q_e = Adsorption capacity at equilibrium, mg/g

k_1 = First order rate constant, min^{-1}

t = time, min

2.12.4 Pseudo Second-Order Kinetic Model

PSO kinetic model considers the uptake rate of adsorbate to be directly proportional to the number of active adsorbent sites. Unlike PFO, PSO describes the adsorption of solute onto adsorbent based on the second-order reaction rate. The PSO kinetic model can be expressed in curvilinear and linear form using Equations 2.10 and 2.11, respectively.

$$\frac{dq_t}{dt} = k_2(q_e - q_t)^2 \quad (2.10)$$

Where;

q_t = Amount of anionic surfactant on PAC/PUF at time t , mg/g

q_e = Adsorption capacity at equilibrium, mg/g

k_2 = Second order rate constant, min^{-1}

t = time, min

Equation 2.10 can be integrated for t (0,t) and q_t (0, q_t). The resulting POS model in linear form can be obtained as follows:

$$\frac{t}{q_t} = \frac{1}{k_2 q_e^2} + \frac{t}{q_e} \quad (2.11)$$

$$\frac{1}{q_t} = \frac{1}{k_2 q_e^2} \left[\frac{1}{t} \right] + \frac{1}{q_e} \quad (2.12)$$

$$q_t = q_e - \left[\frac{1}{k_2 q_e} \right] \left[\frac{q_t}{t} \right] \quad (2.13)$$

$$\frac{q_t}{t} = k_2 q_e^2 - k_2 q_e q_t \quad (2.14)$$

Four different linear forms of the PSO model resulted. However, Equation 2.11 provides the best fit of kinetic data among the others as it has a better distribution of errors on the curve (Kajjumba et al., 2018).

CHAPTER 3

METHODOLOGY AND WORK PLAN

3.1 Introduction

All methodologies required to carry out the study are included in this chapter. For instance, the synthesis of PAC/PUF adsorbent, characterization work of PAC/PUF adsorbent, preparation of dye solution, optimization of adsorption experiment, and modelling of adsorption isotherm and kinetics. The materials and chemicals used throughout the study are listed as well. A complete methodology flowchart is presented in Figure 3.1 to showcase the overall process flow of the study.

3.2 Materials and Chemicals

Table 3.1 presents all the specifications of the materials and chemicals used in the study. Congo Red (CR), an azo dye frequently present in textile wastewater, was used in the study.

Table 3.1: Specifications of Materials and Chemicals Used.

Chemicals	Purity (%)	Brand/Source	Purpose
Acetone	99.5	Synerlab	Remove PUF impurities and prepare PAC solution
Congo Red	≥ 97.0	Merck	Model pollutant
Deionised water	-	UTAR Lab	Dilution
Ethanol	95.0	Synerlab	Eluent
HCl	37.0	Sigma-Aldrich	pH adjuster
NaOH	≥ 99.0	Synerlab	pH adjuster
NaCl	≥ 99.5	Merck	Zeta potential analysis
PAC	-	R&M	Adsorbent
PUF	-	Hardware Store	Adsorbent support

3.3 Equipment

All the specifications of the instruments used in the experiment are listed in Table 3.2.

Table 3.2: Instruments Used in the Experiment.

Instrument	Model	Purpose
FTIR	Nicolet iS10	To characterize the functional group
SEM-EDX	Hitachi SEM Model S-3400N	To characterize the surface morphology
Sonicator	WiseClean WUC A03H	Dispersion and mixing of PAC in solution
UV-Vis Spectrophotometer	Varian, Cary 100	To measure dye concentration
Incubator Shaker	Daihan Labtech LSI-3016A	Uniform mixing of PAC/PUF and CR
XRD	Shimadzu XRD-6000	To characterize the crystallinity nature
Oven	Memmert UFB500	To dry PAC/PUF

3.4 Methodology Flow Chart

The overall process flow of the experiment is summarized and illustrated in Figure 3.1. Firstly, PAC/PUF adsorbent was synthesized and characterized. After that, the CR stock solution and calibration curve were prepared. Optimization of the experiment using Respond Surface Methodology (RSM) was carried out to study how different adsorption parameters such as pH, contact time, and initial concentration of dye affect the adsorption efficiency of CR. Characterizations of adsorbents which include PAC/PUF and blank PUF were conducted after adsorption experiments. Isotherm and kinetic studies were performed to analyze the interactions between the dye and the PAC/PUF and determine the kinetic order of the adsorption.

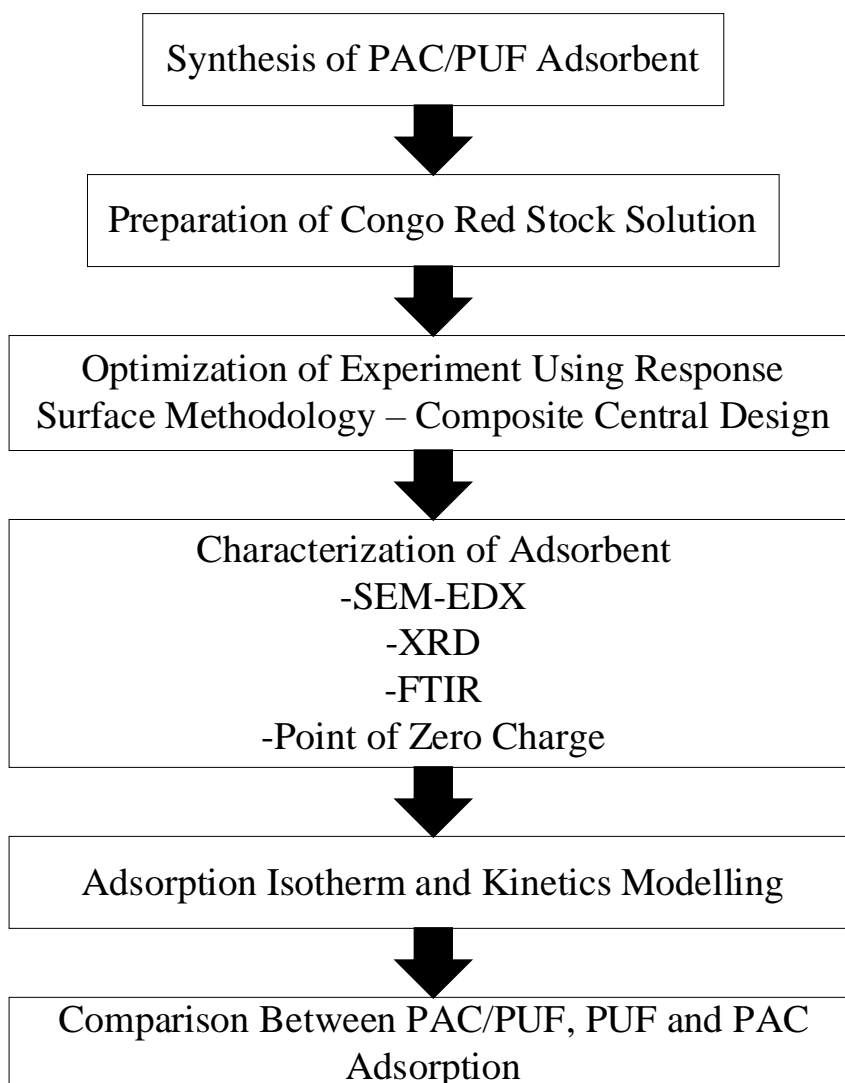


Figure 3.1: Methodology Flow Chart

3.5 Synthesis of PAC/PUF Adsorbent

The raw materials needed were PAC, PUF, and acetone. Firstly, the PAC solution was prepared by sonicating 450 mg of PAC in 100 ml ethanol for 30 min using the WiseClean WUC A03H sonicator. It was thoroughly mixed to ensure the stability and homogeneous dispersion of PAC in the solution. Meanwhile, the PUF was cut into a few cubic shapes with a dimension of (2.0 cm length \times 2.0 cm width \times 2.5 cm height) and immersed into an acetone solution to be sonicated for 15 min. This step was to remove any impurities found in the PUF. After that, the cleaned PUF was taken out from the sonicator and placed in a 70 °C oven to dry for 1 hour. The resultant PUF was left to cool and stored in a beaker when not in use. To support PAC onto PUF, the cooled PUF was fully dipped into the PAC solution for 20 min under

constant stirring. Finally, the synthesized adsorbent PAC/PUF was dried at 80 °C in the oven for 120 min. Figure 3.2 shows the support process of PAC onto PUF. A desiccator was used to keep the dried PAC/PUF until further use (Singh and Vaish, 2019).

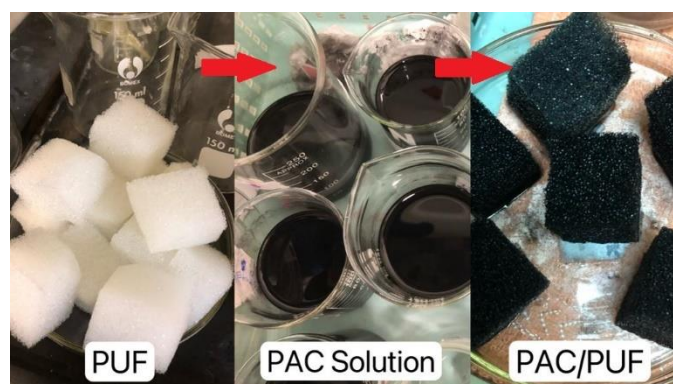


Figure 3.2: Synthesis of PAC/PUF.

3.6 Preparation of Congo Red Stock Solution

Preparation of CR stock solution was done by mixing 0.06 g of CR dye with 1000 mL of deionized water to obtain an initial dye concentration of 60 mg/L. The stock solution was diluted to different concentrations of 10 mg/L, 20 mg/L, 30 mg/L, 40 mg/L, and 50 mg/L to obtain standard solutions for calibration curve plotting. A UV-Vis spectrophotometer was utilized to measure the dye concentration at a wavelength of 497 nm (Rajoriya et al., 2021).

3.7 Characterisation of Adsorbents

SEM analysis was carried out to study the surface morphologies of the blank PUF and PAC/PUF by scanning the adsorbents samples using highly concentrated electron beams. The samples were coated with a thin layer of gold before SEM analysis. SEM micrographs were captured at various magnifications using a current intensity of 30.0 mA and an accelerating voltage of 40.0 kV. At the same time, the elemental composition of the blank PUF and PAC/PUF was investigated using EDX analysis. Both analyses were done using Hitachi SEM Model S-3400N.

FTIR analysis was conducted to determine the functional groups of PAC/PUF. The instrument used for this experiment was Nicolet iS10. By merely scanning the sample of PAC/PUF using infrared light, FTIR analysis will produce an adsorption band. Any changes in the typical pattern of the bands indicated a modification in the composition of the PAC/PUF. In this experiment, FTIR was performed at resolution of 4 cm^{-1} , 64 scans, and spectrum range of $400\text{ to }4000\text{ cm}^{-1}$.

Besides, XRD analysis was conducted to verify the crystallinity or amorphous nature of the PAC/PUF adsorbent. A copper radiation source at a voltage of 40 kV and a current of 30 mA was used to perform the XRD. The scan range specified was 10° to 80° , with a scan speed of $2^\circ/\text{min}$ and a sampling pitch of 0.02° . The analysis was performed using the Shimadzu XRD-6000 model.

3.8 Adsorption Experiment

Synthesized PAC/PUF was added into 100 mL of CR solution of different initial concentrations of dye (20-60 mg/L) and pH (3.5-10.5) for a contact time between 60 to 180 min. Figure 3.3 shows the CR solutions at different concentrations and pH. The mixtures were placed in 250 mL conical flasks. All the adsorption experiments were carried out in a shaking incubator at a rotation speed of 200 rpm. After adsorption, the CR solutions were centrifuged and the supernatants were subjected to a concentration test using a UV-Vis spectrophotometer at a wavelength of 497 nm.

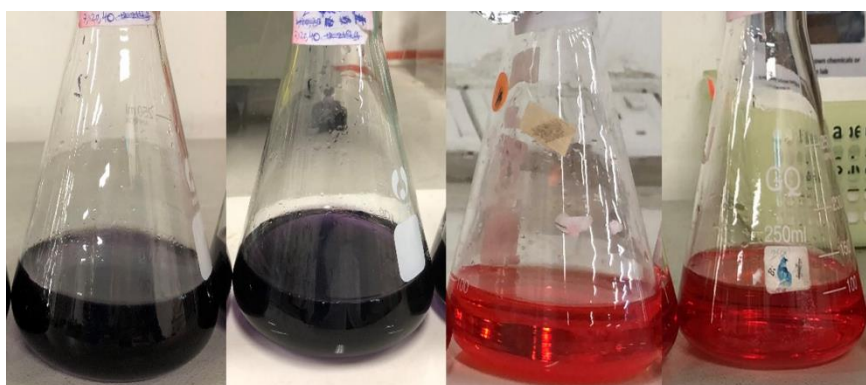


Figure 3.3: Congo Red Solutions at Different Concentrations and pH.

3.9 Design of Experiment

Response Surface Methodology was used to examine the interaction between the three independent variables that impact the adsorption efficiency of CR onto PAC/PUF. The three variables were pH (X_1), contact time (X_2), and initial concentration of dye (X_3). The response variable was the adsorption efficiency of PAC/PUF.

The ranges and coded levels of variables were decided based on the literature findings in Chapter 2. Thus, 5 levels of -2, -1, 0, 1, 2 were coded as shown in Table 3.3. Based on the central composite design (CCD) model generated, a total of 20 experimental runs were needed. The total run could be calculated based on Equation 3.1. Table 3.4 shows the experiment matrix generated by the CCD model. Based on these randomized experimental runs, adsorption experiments were conducted to obtain the adsorption efficiency.

$$Total\ run = 2^n (factorial) + 2n (axis) + 6 (center) \quad (3.1)$$

Table 3.3: Range of Actual Values and Coded Levels for Each Variable.

Variables	Code	Ranges and Coded Levels				
		$-\alpha$ (-2)	-1	0	1	α (+2)
pH	X_1	3.5	5.25	7	8.75	10.5
Contact Time (min)	X_2	60	90	120	150	180
Initial Concentration of Dye (mg/L)	X_3	20	30	40	50	60

Table 3.4: Experimental Design Matrix of CCD Coded Variables.

Run	X_1 : pH	X_2 : Contact Time (min)	X_3 : Initial Concentration (mg/L)
1	7	60	40
2	3.5	120	40
3	5.25	90	30
4	5.25	150	30
5	10.5	120	40

Table 3.4 (Continued)

Run	X₁: pH	X₂: Contact Time (min)	X₃: Initial Concentration (mg/L)
6	8.75	150	50
7	7	120	40
8	8.75	150	30
9	7	120	40
10	7	120	60
11	7	120	20
12	5.25	150	50
13	5.25	90	50
14	7	120	40
15	8.75	90	50
16	7	180	40
17	7	120	40
18	7	120	40
19	7	120	40
20	8.75	90	30

3.10 Determination of Adsorption Efficiency and Capacity

The adsorption efficiency was calculated based on Equation 3.2 (Hazman Hasan, Fatin Mohd Razali and Shazali Mhd Shah, 2022). In addition, both adsorption capacity at equilibrium and adsorption capacity at time t were calculated using Equations 3.3 and 3.4, respectively (Singh and Vaish, 2019).

$$Removal (\%) = \frac{(C_0 - C_f)}{C_0} \times 100\% \quad (3.2)$$

Where;

C_0 = Initial concentration of CR, mg/L

C_f = Final concentration of CR, mg/L

$$q_e = \frac{(C_0 - C_e)V}{w} \quad (3.3)$$

Where;

q_e = Adsorption capacity at equilibrium, mg/g

C_e = Concentration of dye at equilibrium, mg/L

V = Volume of CR solution, L

w = Mass of PAC/PUF, g

$$q_t = \frac{(C_0 - C_t)V}{w} \quad (3.4)$$

Where;

q_t = Adsorption capacity at time, t , mg/g

C_t = Concentration of CR at time, t , mg/L

3.11 Isotherm and Kinetic Study

The isotherm and kinetics for the adsorption of CR were analyzed by investigating whether the adsorption data could best fit the PFO or PSO kinetic models and the Langmuir and Freundlich isotherm models. The isotherm and kinetic models are presented in Table 3.5.

Table 3.5: Isotherm and Kinetic Adsorption Models.

Model	Formula
Langmuir Isotherm	$q_e = \frac{q_o K_L C_e}{1 + K_L C_e}$
Freundlich Isotherm	$q_e = b C_e^{\frac{1}{n}}$
PFO	$\frac{dq_t}{dt} = k_1 (q_e - q_t)$
PSO	$\frac{dq_t}{dt} = k_2 (q_e - q_t)^2$

3.11.1 Adsorption Isotherm

Langmuir and Freundlich isotherm models as listed in Table 3.5 were applied to best fit the experimental results. Also, the adsorption favourability was checked using the separation factor listed in Equation 2.5. Then, the Langmuir and Freundlich equations were translated into graphical representation using Equations 2.4 and 2.7, respectively.

3.11.2 Adsorption Kinetic

The adsorption rate was investigated by fitting the experimental results to PFO and PSO. The PFO and PSO models used were presented in Table 3.5. Then, the PFO and PSO equations were translated into graphical representation using Equation 2.9 and Equation 2.11, respectively.

CHAPTER 4

RESULTS AND DISCUSSION

4.1 Characterization

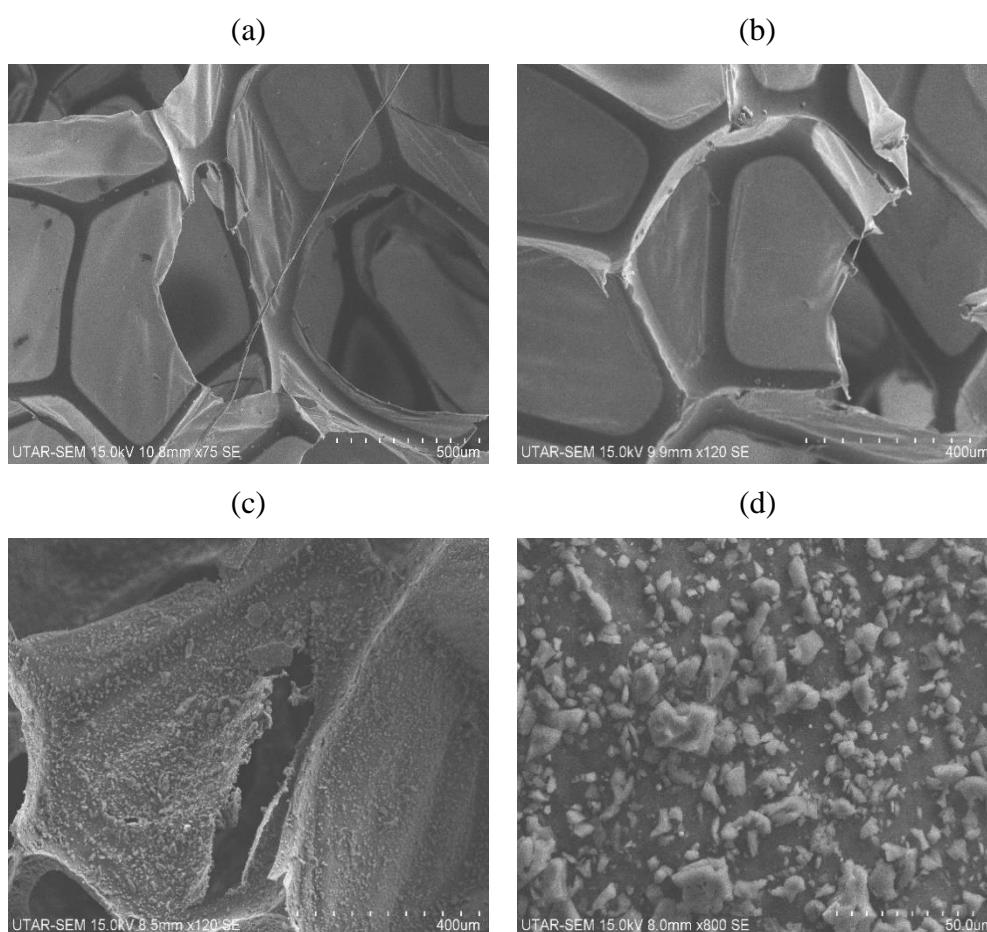
SEM-EDX, XRD, and FTIR were used to characterize the blank PUF and PAC/PUF. This characterization analysis enabled the study of their surface morphology, composition, amorphous or crystallinity nature, and functional groups. The point of zero charge was conducted to examine the surface charges of PAC/PUF.

4.1.1 SEM-EDX

The surface morphologies of blank PUF and PAC/PUF were examined using SEM, and the images are presented in Figure 4.1. It was observed that all the SEM images depicted the microstructure of open-cell chains, where the cavities were shaped like dodecahedrons. These cavities were classified based on how the internal pore strain was distributed and linked (Bouraie and Abdelghany, 2020). Figure 4.1 (a-b) show a porous network structure of blank PUF with a pore size of 400 μm to 500 μm , which was aligned with the result obtained by Li et al. (2016), where the pore size must be in between the range of 100 μm to 700 μm to maintain a high adsorbate capacity. It also revealed a clean and smooth skeleton surface.

In Figure 4.1 (c-d), the skeleton structure of PAC/PUF before adsorption remained intact, demonstrating a strong binding between the open dodecahedral cavities that would not damage even during the ultrasonic dip-coating process to load the PAC onto PUF. However, the surfaces of PAC/PUF were no longer smooth as a dense distribution of PAC completely covered them, proving the coating of PAC onto PUF was feasible and successful. As a result, the microstructure of PUF became rougher, enabling an improved adsorption capacity and enhanced adsorption efficiency (Yuan et al., 2017).

Figure 4.1 (e-f) shows that the SEM images of PAC/PUF after adsorption had no significant change from the PAC/PUF before adsorption. Similar results were obtained by Zhao et al. (2021) and Lefebvre et al. (2018), whereby dyes such as Rhodamine B, Methylene Blue, and Crystal Violet adsorbed onto polyurethane foam were not visible under SEM analysis. The reason may be due to the extremely fine particles of CR and the inefficiency of the SEM equipment in detecting the CR particles. Thus, another characterization method, such as EDX was analyzed to check for the presence of CR.



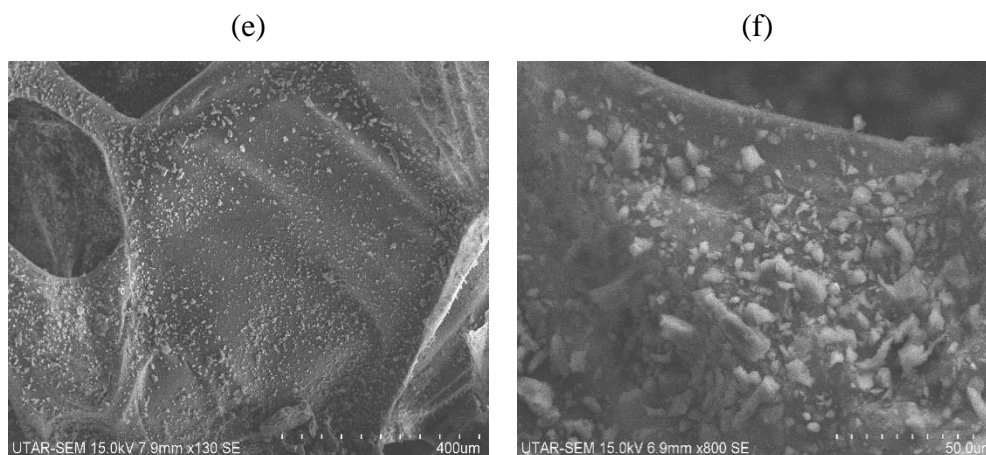


Figure 4.1: SEM Images of Blank PUF (a, b), PAC/PUF Before Adsorption (c,d) and PAC/PUF After Adsorption (e,f) with Different Magnifications.

The EDX results of blank PUF, PAC/PUF before adsorption, and PAC/PUF after adsorption are shown in Table 4.1. The ultimate purpose of EDX was to determine the presence of CR elements in the PAC/PUF after adsorption. PUF is composed of C, H, N, and O basic elements while commercial PAC mainly consists of C element with some impurities such as Cl, Cu, and Zn. On the other hand, CR compound consists of Na and S elements with other common C, H, N, and O elements. Therefore, the results showed that the total content of Na and S found in PAC/PUF after adsorption increased from 0.00 wt% to 0.64 wt% and 0.00 wt% to 0.40 wt%, respectively. This result indicated the successful presence and adsorption of CR onto PAC/PUF during the adsorption experiments.

Besides Na and S, carbon and oxygen are the predominant elements on the surface of powdered activated carbon, with carbon having a greater ratio than oxygen (Alam et al., 2021). The carbon weight percentage after adsorption was 71.40 wt%, which was higher than oxygen at 18.08 wt%. The Cl element was one of the impurities found in the PAC.

Table 4.1: EDX Results of Various Adsorbents.

Adsorbents	C		O		N		Na		S		Cl	
	Wt. (%)	At. (%)	Wt. (%)	At. (%)	Wt. (%)	At. (%)	Wt. (%)	At. (%)	Wt. (%)	At. (%)	Wt. (%)	At. (%)
PUF	63.10	68.63	26.15	21.35	10.74	10.02	-	-	-	-	-	-
PAC/PUF Before Adsorption	63.54	69.05	25.08	20.46	11.16	10.40	00.00	00.00	00.00	00.00	00.23	00.08
PAC/PUF After Adsorption	71.40	76.39	18.08	14.52	09.26	08.50	00.64	00.36	00.40	00.16	00.23	00.08

4.1.2 XRD

The XRD results of blank PUF, PAC/PUF before adsorption, and PAC/PUF after adsorption are shown in Figure 4.2. Based on the results, PUF had a broad peak at a 2θ value of 20.54° , similar to the XRD pattern obtained by Liu et al. (2016). This hunchback characteristic pattern is typically associated with materials with low crystallinity. Thus, it could be confirmed that the PUF used in this work was amorphous, similar to the findings done by Dias et al. (2010).

However, the XRD pattern of PAC/PUF before adsorption revealed a distinct difference with the blank PUF, especially around the 2θ values ranging from $10-25^\circ$ and 40° . The hunchback characteristic at $10-25^\circ$ was more prominent than blank PUF. The resultant difference was due to the increased intensity caused by the loading of PAC onto PUF. It was found that the intensity increased from 166 cps to 216 cps when PAC was loaded to PUF. Commonly, the 2θ value of PAC falls around 23° , corresponding to the Bragg's reflection plane of (002) (Sharma et al., 2019). A previous study also found that PAC had a diffraction peak around 43° , corresponding to the reflection plane of (100) (Omri and Benzina, 2012). It is known to have an XRD pattern peculiar to the ones of amorphous material. Thus, based on Figure 4.2, the diffraction peaks at these 2θ areas were higher, suggesting the successful attachment of PAC onto PUF.

According to AlAbdulaal et al. (2022), the XRD pattern of Congo Red showed diffraction peaks at 2θ values of around 37.84° , 44.91° , and 45.33° that corresponded to (117), (124), and (134) planes, respectively. Compared with PAC/PUF before adsorption, the XRD pattern obtained by PAC/PUF after adsorption possessed a sharp increase in the intensity at these peaks. For instance, at $2\theta = 38.32^\circ$, the intensity before adsorption was 65 cps and increased to 76 cps after adsorption. Also, at $2\theta = 44.58^\circ$, the intensity of 64 cps rose to 82 cps after adsorption. The increment reflected the effective attachment of CR onto PAC/PUF and the significance of acidic dye solution condition to create more active sites on the PAC/PUF for good adsorption.

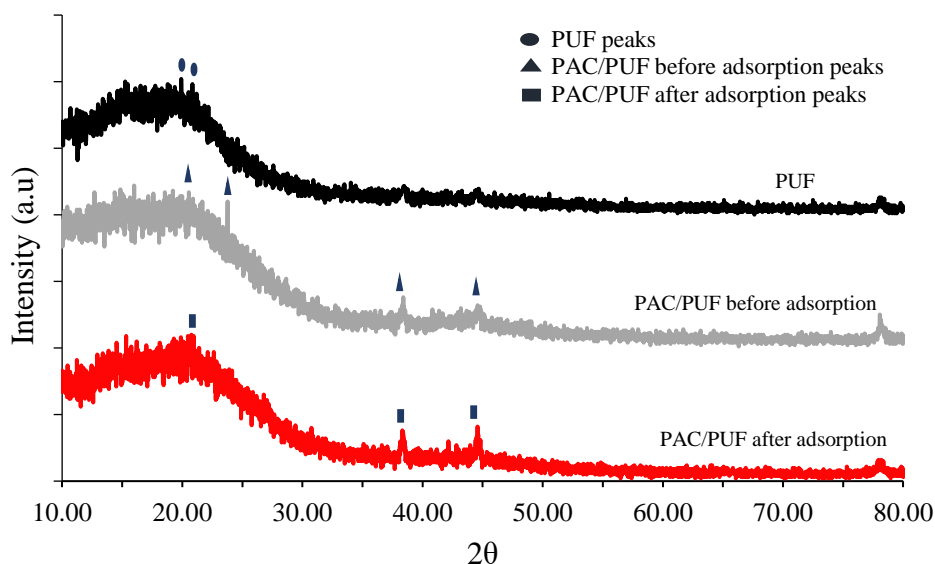


Figure 4.2: XRD Results of Blank PUF and PAC/PUF Before and After Adsorption.

4.1.3 FTIR

The FTIR spectra of Congo Red, blank PUF, PAC/PUF before, and PAC/PUF after adsorption are illustrated in Figure 4.3 – Figure 4.5. The FTIR spectroscopic analysis of PUF showed a peak at 3284 cm^{-1} corresponds to N-H stretching vibration. This peak verified the presence of secondary amine groups in PUF. The peaks at 2969.64 cm^{-1} , 2925.89 cm^{-1} , and 2862.83 cm^{-1} were caused by C-H stretching vibrations of CH_2 groups (Kraitape and Thongpin, 2016). Similar findings were reported in another study by Rastegarfar, Behrooz and Barikani (2018). Besides, C=O stretching vibration of the urethane bond was found at the peak of about 1714.83 cm^{-1} . The transmittance band at 1638 cm^{-1} , 1595.99 cm^{-1} , and 1219.37 cm^{-1} were attributed to the N-H bending and N-C bond in urethane linkages. The presence of C-O was determined at a wavenumber of 1100 cm^{-1} . These results aligned with the study done by Caddeo et al. (2015). Figure 4.4 shows the FTIR spectrum of PUF.

The FTIR spectra of CR in Figure 4.3 shows a peak at 3470 cm^{-1} due to the N-H stretching vibration of primary amine. Aromatic C=C stretching vibration was also present due to the visible peak at 1582 cm^{-1} . Other peaks at 1446 cm^{-1} , 1347 cm^{-1} , and 1063 cm^{-1} proved the existence of N=N, C-N bending, and S=O of sulfonic acid stretching vibrations (Moon et al., 2018).

It could be observed that the FTIR spectra of PAC/PUF before adsorption significantly differed from blank PUF after the coating of PAC onto the adsorbent. The N-H and C-O peaks at approximately 3284 cm^{-1} and 1100 cm^{-1} became weak and broad in PAC/PUF before adsorption. It was due to several interactions such as H-bonding between the PAC and the PUF. Thus, it could be proven that PAC was present on the surface of the PUF and became successfully adsorbed (Keshavarz et al., 2016). Other noticeable peaks at approximately 1638 cm^{-1} and 1100 cm^{-1} of PUF had become broader and shifted to 1525 cm^{-1} and 1080 cm^{-1} , respectively in PAC/PUF before adsorption. All these changes suggested the interactions between the functional groups of the PAC and the PUF.

As shown in Figure 4.5, the FTIR spectra of PAC/PUF before and after adsorption had similar characteristics, with some peaks being shifted and intensity increased. For instance, the adsorption band at 3255 cm^{-1} caused by the N-H stretching vibration increased to 3260 cm^{-1} , and intensity increased to 87 % from 81 %. In addition, the PAC/PUF before adsorption had a peak at 2846 cm^{-1} , which was assigned to the C-H stretching band. This peak was increased to 2859 cm^{-1} after adsorption. Also, the PAC/PUF before adsorption showed another peak at 1525 cm^{-1} caused by the stretching vibration of C=C in aromatic rings. After adsorption, this peak was increased to 1529 cm^{-1} . According to Bilir et al. (2013), all these increments were due to the adsorption of dye onto the foam. However, the changes in the FTIR spectra after adsorption was not significant, suggesting no bonds were formed or broken after adsorption and that physical adsorption might had taken place.

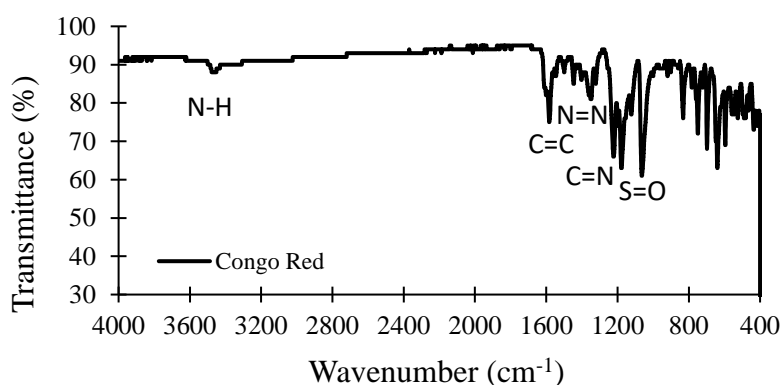


Figure 4.3: FTIR Spectra of Congo Red.

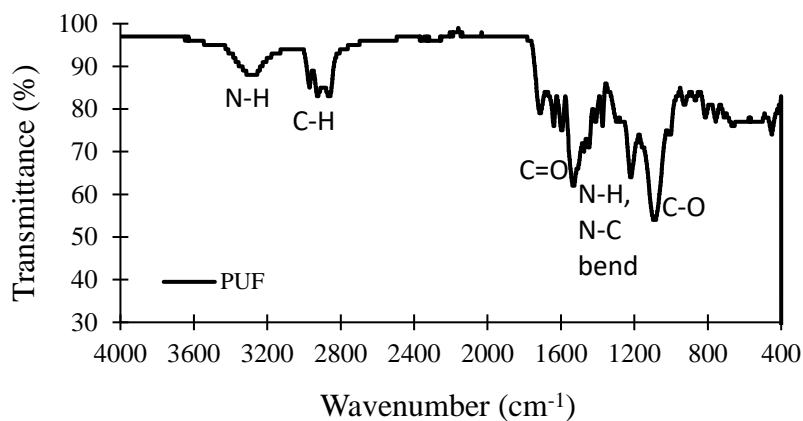


Figure 4.4: FTIR Spectra of PUF.

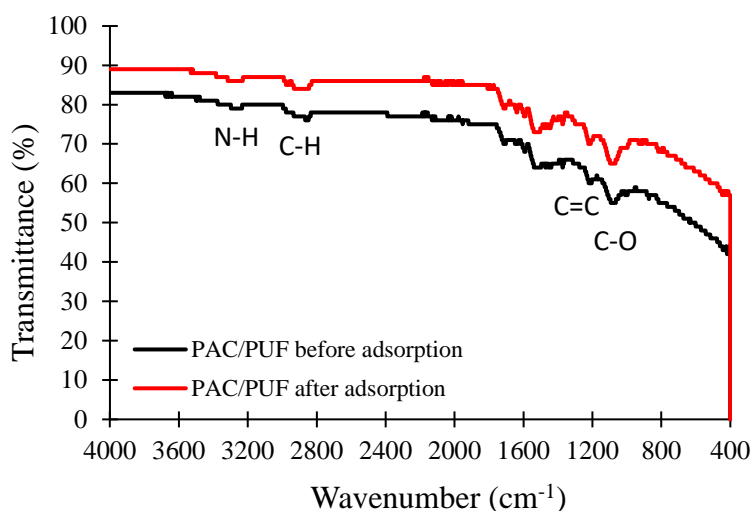


Figure 4.5: FTIR Spectra of PAC/PUF Before Adsorption and PAC/PUF After Adsorption.

4.1.4 Point of Zero Charge

The pH of point of zero charge (pH_{pzc}) of the PAC/PUF was studied using pH drift method. The pH_{pzc} could be determined by locating the point of intersection between the pH_{final} and $\text{pH}_{\text{initial}}$ curves as shown in Figure 4.6. The experimental results showed that the two curves intersected at pH 8, implying the pH_{pzc} of PAC/PUF was pH 8. Therefore, a net positive charge was found on the surface of PAC/PUF below pH 8 and a net negative charge above pH 8. For this reason, the adsorption of CR was more favourable when the dye solution pH was lower than pH_{pzc} as more positive charges were available on the PAC/PUF surfaces. The obtained pH_{pzc} value of pH 8 was consistent with

the study by Adam (2016) that reported a pH_{pzc} of pH 7.8 for commercial activated carbon. According to Prashantha Kumar et al. (2015), the pH_{pzc} of activated carbon was around pH 8.5 when the pH drift method was employed.

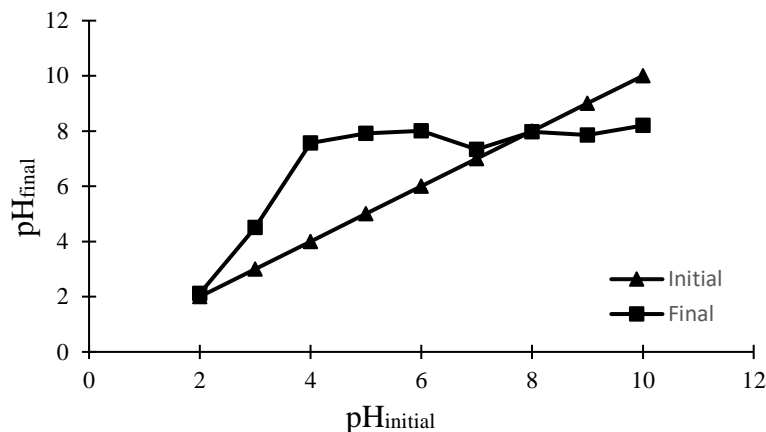


Figure 4.6: Point of Zero Charge of PAC/PUF.

4.2 Statistical Analysis and Optimization Study

RSM using CCD model was utilized to study the relationship between each variable and dye adsorption efficiency.

4.2.1 Regression Analysis

Table 4.2 shows the adsorption efficiency of CR ranged from 48.30 % to 84.65 % in response to the combination of three independent variables pH (X_1), contact time (X_2), and initial concentration of dye (X_3).

Based on Design Expert software, the model obtained for CR adsorption efficiency was significant. The model suggested was quadratic and the empirical relations could be defined by Equation 4.1, where Y is the adsorption efficiency. The positive and negative coefficients indicated the positive and negative effects on the adsorption efficiency.

$$Y = 276.35 - 31.72X_1 - 0.6204X_2 - 3.3315X_3 + 0.01755X_1X_2 + 0.1035X_1X_3 + 0.001304X_2X_3 + 1.54308X_1^2 + 0.002810X_2^2 + 0.025607X_3^2 \quad (4.1)$$

Table 4.2: Adsorption Efficiency Based on Experimental Design Matrix.

Run	Independent Variables			Adsorption Efficiency (%)	
	X ₁ : pH	X ₂ : Contact Time (min)	X ₃ : Initial Concentration (mg/L)	Experimental Values	Predicted Values
1	7	60	40	48.35	50.01
2	3.5	120	40	84.65	86.09
3	5.25	90	30	70.64	70.50
4	5.25	150	30	79.93	81.62
5	10.5	120	40	60.10	58.99
6	8.75	150	50	62.84	62.66
7	7	120	40	52.40	53.64
8	8.75	150	30	63.67	66.29
9	7	120	40	58.55	53.64
10	7	120	60	52.53	55.84
11	7	120	20	74.90	71.92
12	5.25	150	50	72.54	70.74
13	5.25	90	50	61.00	58.05

Table 4.2 (Continued)

Run	Independent Variables			Adsorption Efficiency (%)	
	X ₁ : pH	X ₂ : Contact Time (min)	X ₃ : Initial Concentration (mg/L)	Experimental Values	Predicted Values
14	7	120	40	52.68	53.64
15	8.75	90	50	48.30	46.28
16	7	180	40	78.83	77.50
17	7	120	40	51.86	53.64
18	7	120	40	52.93	53.64
19	7	120	40	53.07	53.64
20	8.75	90	30	50.01	51.48

The analysis of variance (ANOVA) on the experimental values was analyzed and presented in Table 4.3. The analysis was done to justify the accuracy of the model. The model F-value of 31.59 indicated that it was significant and only a 0.01 % chance this value could occur due to noise. Meanwhile, the P-value was used to indicate the probability of the F-value. Commonly, a P-value of 0.05 or less suggests that the model terms are significant, while a P-value of 0.1 or greater suggests otherwise. In this case, X_1 , X_2 , X_3 , X_1^2 , X_2^2 , X_3^2 were all less than 0.05. Thus, they were significant model terms. However, X_1X_2 , X_1X_3 , and X_2X_3 were slightly insignificant, implying that the interaction terms in the adsorption efficiency of CR may not be significant.

On the other hand, the lack of fit F-value of 1.82 implied that the lack of fit was not significant relative to the pure error. This signified that the model terms fitted well to the model. Besides, there was only a 26.34 % chance that a lack of fit F-value this large could occur due to noise.

Table 4.3: ANOVA Results for Congo Red Adsorption Efficiency.

Source	Sum of Squares	Degree of Freedom	Mean Square	F-value	Probability, P-value	
Quadratic Model	2449.84	9	272.20	31.59	< 0.0001	Significant
X_1 – pH	734.27	1	734.27	85.23	< 0.0001	
X_2 – Contact Time	756.11	1	756.11	87.76	< 0.0001	
X_3 – Initial Concentration of Dye	258.49	1	258.49	30.00	0.0003	
X_1X_2	6.79	1	6.79	0.7881	0.3955	
X_1X_3	26.25	1	26.25	3.05	0.1115	
X_2X_3	1.22	1	1.22	0.1421	0.7140	
X_1^2	561.49	1	561.49	65.17	<0.0001	
X_2^2	160.86	1	160.86	18.67	0.0015	
X_3^2	164.86	1	164.86	19.14	0.0014	
Residual	86.15	10	8.62	-	-	
Lack of Fit	55.61	5	11.12	1.82	0.2634	Not significant

Table 4.3 (Continued)

Source	Sum of Squares	Degree of Freedom	Mean Square	F-value	Probability, P-value
Pure Error	30.54	5	6.11	-	-
Corrected Total	2536.00	19	-	-	-

$R^2 = 0.9660$; Adjusted $R^2 = 0.9355$; Predicted $R^2 = 0.7992$; Adequate Precision = 19.1785

Generally, a high coefficient of determination (R^2) of more than 0.90 is desired to show the goodness of fit to the model. Based on the experimental results, the R^2 value of 0.9660 implied that 96.60 % of the data could fit the model well. Furthermore, the adjusted R-squared of 0.9355 suggested that the correlation was 93.55 % reliable when new independent variables were to be added to the model. In the meantime, the predicted value of 0.7992 indicated how well this model would predict responses for new observations. Besides, the adequate precision ratio was 19.178, implying that the model had an adequate signal to navigate the design space.

Figure 4.7 shows the predicted and actual values of the response. Based on the figure, it was proven that most of the actual experimental values aligned with the predicted values, validating that the model suggested was accurate and suitable for predicting the adsorption efficiency of CR.

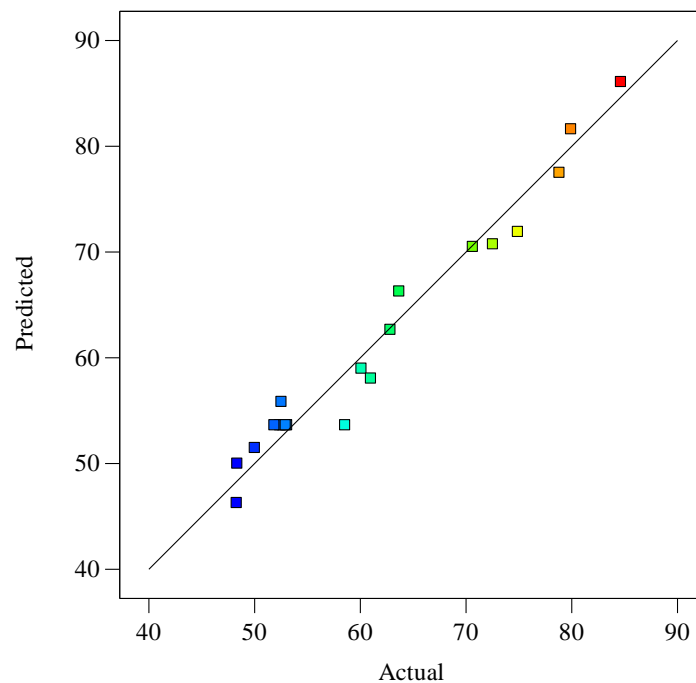


Figure 4.7: Predicted and Actual Values for Adsorption Efficiency of Congo Red.

4.2.2 Response Surface Analysis

Generally, the model term with a higher F-value suggests that the response is more greatly affected by it. Thus, based on the ANOVA results obtained, contact time had the most significant impact on the adsorption efficiency of CR, followed by pH and higher order of pH. The initial concentration of CR brought a lesser effect on the adsorption efficiency of CR. A perturbation plot was presented to better visualize the results of these variables on the removal of CR. Figure 4.8 illustrates the perturbation plot of the variables.

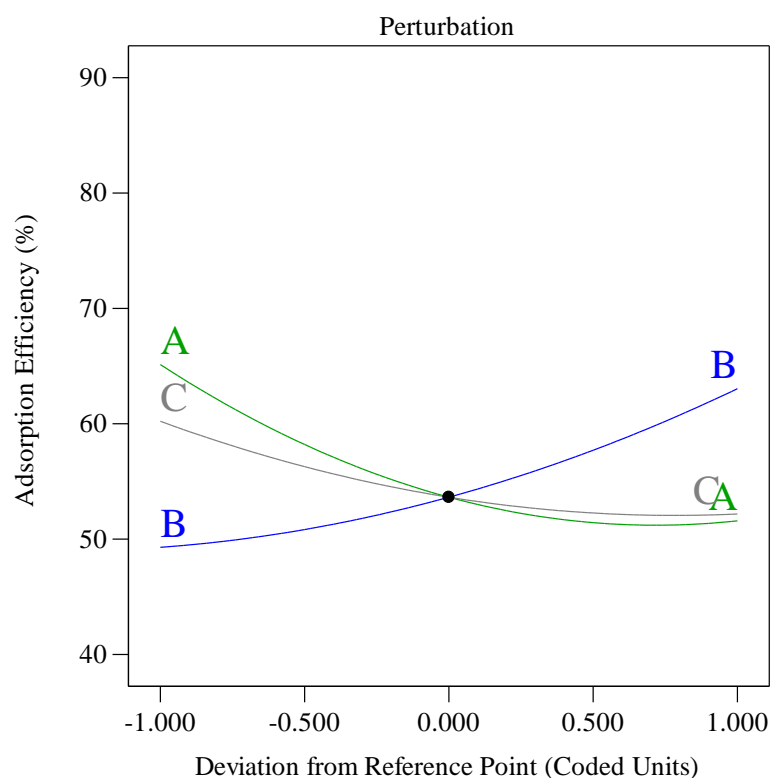


Figure 4.8: Perturbation Plot of Three Independent Variables Affecting Adsorption Efficiency of Congo Red (A = pH; B = Contact Time; C = Initial Concentration of Congo Red).

Based on the perturbation plot, A and B had steep curvatures, which conveyed the strong effects on the adsorption efficiency of CR. In the case of A, the adsorption efficiency decreased with increasing solution pH. However, in the case of B, the adsorption efficiency increased when the contact time increased. For variable C, the adsorption efficiency slightly decreased when the initial concentration of CR increased, implying that the effectiveness of

variable C in removing CR was relatively insignificant. Among these three curvatures observed, curvature for contact time (B) was the steepest. Hence, it had the most significant impact on the adsorption efficiency of CR.

3D surface plots are also presented in Figure 4.9 to demonstrate how the independent variables influenced the adsorption efficiency of CR. Red showed the highest adsorption efficiency, while blue determined the lowest adsorption efficiency.

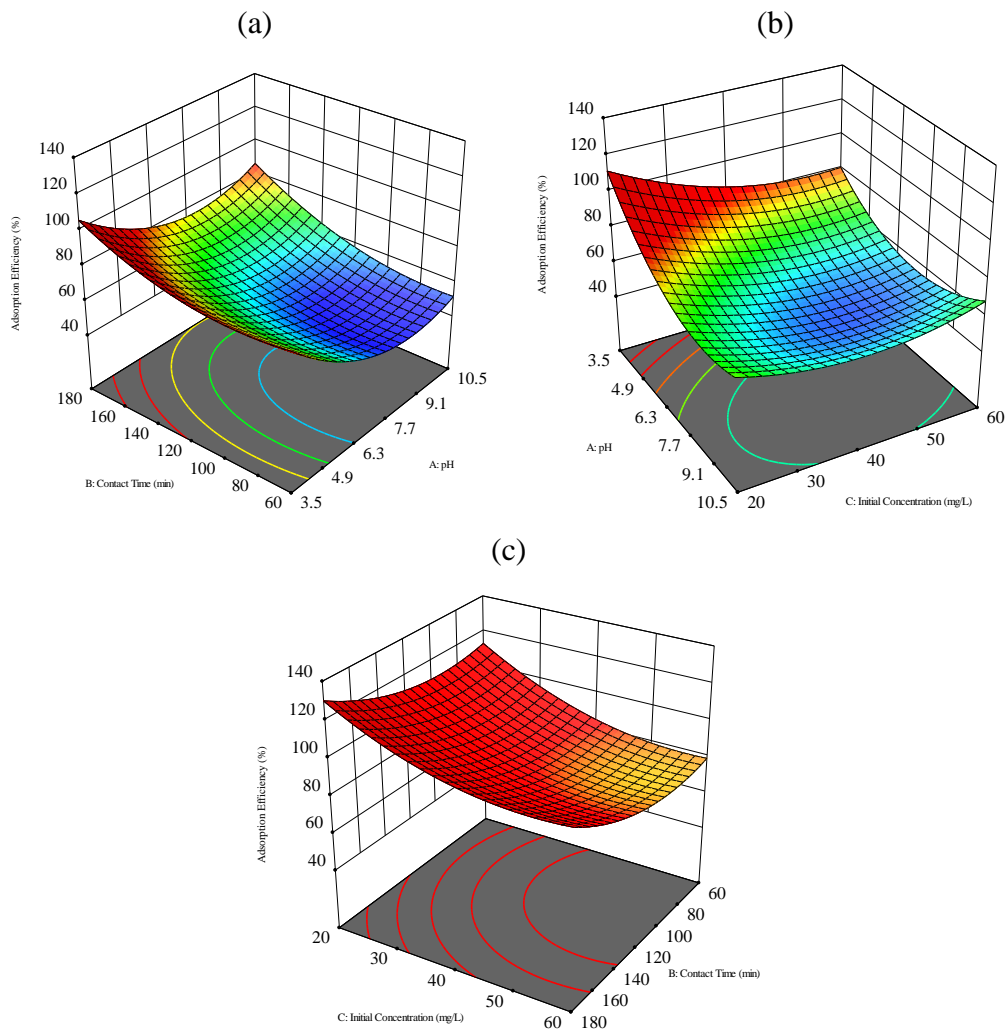


Figure 4.9: Effects of Three Independent Variables Affecting Adsorption Efficiency of Congo Red at Fixed (a) Initial Concentration of 40 mg/L; (b) Contact Time of 120 min; (c) pH of 3.5.

According to Figure 4.9 (a), the adsorption efficiency increased when the contact time increased from 60 min to 180 min and the pH decreased from pH 10.5 to pH 3.5. This behaviour could be due to the abundant active sites available on the PAC/PUF surface for rapid adsorption of CR. Additionally, CR is an anionic dye. It has negative charges that will attract the positive charges particles surrounding them to form strong bonds, also known as an electrostatic attraction. When the dye solution pH dropped from alkali to acidic condition (pH 3.5), there was more H^+ presented on the active sites of the PAC/PUF, resulting in a more positively charged PAC/PUF (Chukwuemeka-Okorie et al., 2021). As a result, the negatively charged CR was electrostatically attracted to the PAC/PUF and the removal efficiency increased. This behaviour aligned with the findings from other experimental runs, such as run 1, run 2, and run 9. It could be observed that when the contact time increased from 60 min (run 1) to 120 min (run 9) at a fixed concentration of 40 mg/L and pH 7, the adsorption efficiency increased from 48.35 % to 58.55 %. Meanwhile, when the pH decreased from pH 7 (run 9) to pH 3.5 (run 2) at fixed contact time and initial concentration of dye, the adsorption efficiency increased from 58.55 % to 84.65 %.

Furthermore, Figure 4.9 (b) shows the interaction between pH and the initial concentration of CR. It could be noted that a low initial concentration of CR and low pH conditions could result in an increased adsorption efficiency. This was because of the electrostatic attraction between the dye and the H^+ on the active sites of PAC/PUF. Increased adsorption efficiency could also be attributed to the availability of vacant sites on the PAC/PUF when the initial concentration of dye was low. If the vacant sites on the PAC/PUF were fully saturated, the adsorption rate became slow, resulting in the quick attainment of adsorption equilibrium at an early stage (Uddin and Nasar, 2020). Thus, any further increase in the concentration of CR will not increase the adsorption efficiency as proven in run 4 and run 12. The adsorption efficiency decreased from 79.93 % to 72.54 % when the initial concentration of CR increased from 30 mg/L (run 4) to 50 mg/L (run 12).

A similar result was obtained by Yusuff (2019) who reported the adsorption efficiency of chromium using activated carbon decreased when the initial chromium concentration increased from 50 to 250 mg/L. It was believed that the amount of accessible active sites on the activated carbon was still the same even though the initial concentration of chromium increased, causing saturation of active sites on the activated carbon.

Lastly, the impact of contact time on adsorption efficiency became more evident upon examining Figure 4.9 (c), which depicted how the interaction between contact time and initial concentration could result in high adsorption efficiency even though the effect of initial concentration was minimal.

4.2.3 Optimization and Model Validation

Process optimization and model validation were carried out and their outcomes are summarized in Table 4.4. The optimization function embedded in Design Expert software generated several optimal solutions sorted according to their desirability. Three solutions with different combinations were chosen to perform the adsorption experiments. The adsorption experiment for each combination was repeated three times to get average data. Based on Table 4.4, the experimental values on removing CR demonstrated a deviation of less than 2 % from the predicted values. Therefore, the results obtained through experiments were consistent with the predicted values generated by the model, indicating that the RSM technique was an effective method to optimize the adsorption capacity of CR.

Table 4.4: Experimental Versus Predicted Values of the Adsorption Efficiency of Congo Red.

Solution No.	pH	Contact Time (min)	Initial Concentration of Congo Red (mg/L)	Experimental Adsorption Efficiency Values (%)	Predicted Adsorption Efficiency Values (%)	Deviation (%)
1	3.854	137.551	33.566	89.859	90.602	0.82
2	4.089	151.625	39.404	86.896	87.831	1.06
3	5.057	122.484	21.952	85.848	86.645	0.92

4.3 Adsorption Model

The adsorption experiment results were assessed using Langmuir and Freundlich isotherm models. On the other hand, the adsorption kinetics were evaluated using PFO and PSO kinetic models. The optimum adsorption conditions were used for the modelling, which included pH = 3.584, contact time = 60 – 300 min, and initial concentration of dye solution = 33.566 mg/L.

4.3.1 Kinetic Model

Figure 4.10 illustrates the adsorption kinetics of CR onto PAC/PUF. The dye adsorption increased gradually with increasing time until equilibrium was reached within 150 min. The highest adsorption capacity of PAC/PUF was 11.56 mg/g. The adsorption kinetics were further explored using PFO and PSO models. Table 4.5 tabulated the data required for PFO and PSO modelling. Based on Figure 4.11 and Figure 4.12, the linear correlation coefficient (R^2) for the PFO and PSO were 0.8502 and 0.9988, respectively. The high R^2 value validated the suitability of using the PSO kinetic model to describe the adsorption of CR. Besides, the experimental value as shown in Table 4.6 shows that the adsorption capacity at equilibrium (q_e) (~11.56 mg/g) was nearly similar to the theoretical value calculated by PSO (12.1951 mg/g). Hence, it could be stated that the ability of PAC/PUF to adsorb CR was a result of chemical adsorption, which was primarily brought about by the interaction between the surface functional groups of the PAC/PUF and the dye (Yang et al., 2017).

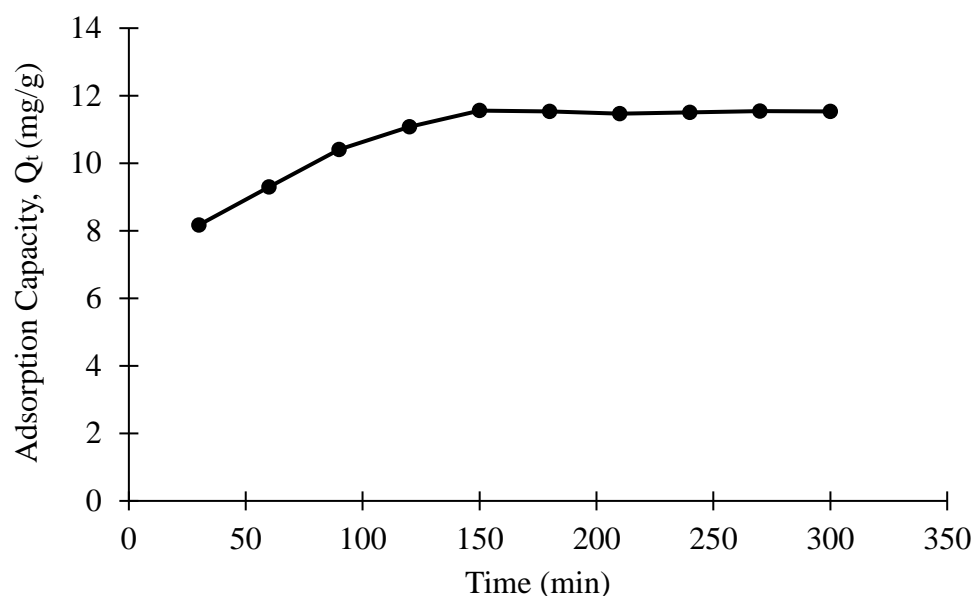


Figure 4.10: Adsorption Kinetic Plot of Congo Red on PAC/PUF at Fixed Conditions (pH = 3.854 and Initial Concentration of Dye = 33.566 mg/L).

Table 4.5: Data for Pseudo-First and Pseudo-Second Order Modelling.

Time (min)	Concentration at Different Times, C_t (mg/L)	Weight of Adsorbent, W (g)	Adsorption Capacity, q_t (mg/g)	$\ln(q_e - q_t)$	t/q_t
30	12.2353	0.261	8.1727	1.2195	3.6708
60	9.2980	0.261	9.2981	0.8154	6.4530
90	6.3976	0.261	10.4093	0.1387	8.6461
120	4.6388	0.261	11.0832	-0.7447	10.8272
150	3.3994	0.261	11.5581	N/A	12.9779
180	3.4588	0.261	11.5353	-3.7826	15.6043
210	3.6353	0.261	11.4677	-2.4038	18.3123
240	3.5411	0.261	11.5038	-2.9129	20.8627
270	3.4424	0.261	11.5416	-4.1072	23.3936
300	3.4565	0.261	11.5362	-3.8230	26.0051

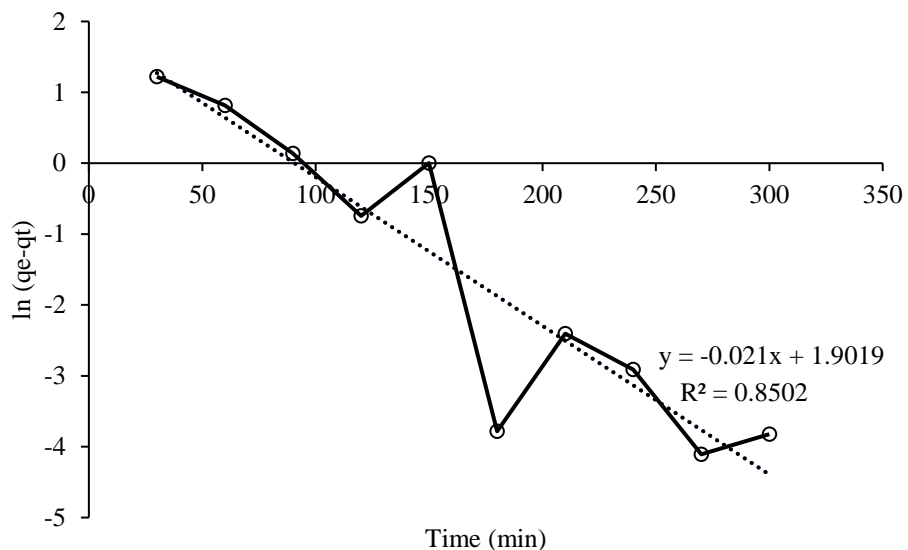


Figure 4.11: Pseudo-First Order Kinetic Plot.

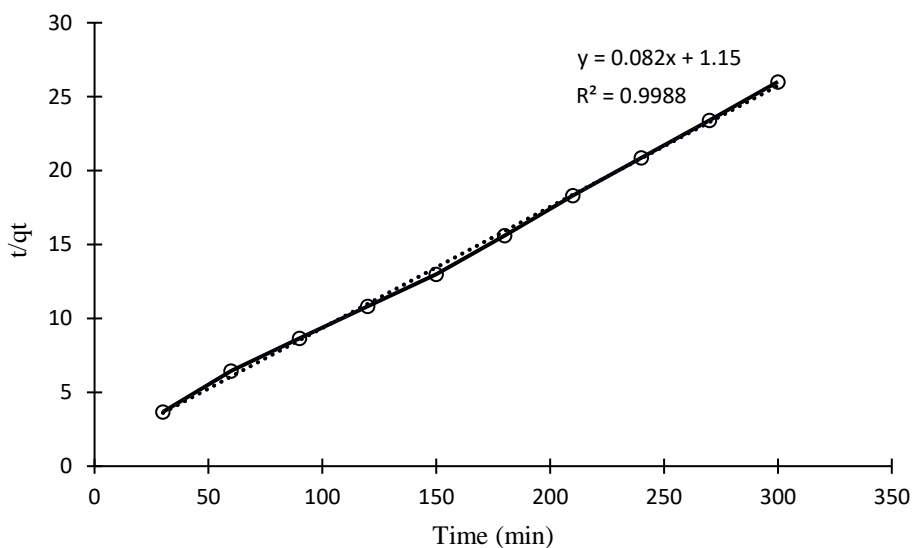


Figure 4.12: Pseudo-Second Order Kinetic Plot.

Table 4.6: Parameters and Constants for Kinetic Modelling.

Model	K_1 (min^{-1})	K_2 (min^{-1})	q_e (mg/g)
Pseudo-First Order	0.021	-	6.6986
Pseudo-Second Order	-	0.005847	12.1951

4.3.2 Isotherm Model

Table 4.7 presents the data required for Langmuir and Freundlich modelling. Based on Figure 4.13 and Figure 4.14, the linear correlation coefficient (R^2) for Langmuir and Freundlich were 1.000 and 0.963, respectively. This showed the suitability of both models to describe the adsorption equilibrium of CR by PAC/PUF. However, the Langmuir isotherm model for CR adsorption was preferred over Freundlich since its R^2 value was ideal and higher than Freundlich. Besides, the separation factor (R_L) shown in Table 4.8 indicated that the adsorption of CR was favourable since the R_L value was between 0 and 1.

Based on the result, it was suggested that the active sites on the surface of PAC/PUF were homogeneous, and the static adsorption of CR on PAC/PUF was a single-layer adsorption. Furthermore, it was assumed that there were no lateral interactive effects between adjacent adsorbed CR molecules. Additionally, each active sites on the surface of PAC/PUF only adsorb one specific CR molecule (Sahoo and Prelot, 2020). Thus, it explained why the adsorption efficiency of CR decreased when more concentration of dyes in the solution increased. Any further increase in the dye concentration will no longer be adsorbed onto its surface.

Table 4.7: Data for Langmuir and Freundlich Modelling.

Time, t (min)	Concentration at Different Times, C_t (mg/L)	Weight of Adsorbent, W (g)	Adsorption Capacity, q_t (mg/g)	C_e/q_e (g/L)	lnq_e (mg/g)	lnC_e (mg/L)
30	12.2353	0.261	8.1727	1.0586	2.1008	2.5043
60	9.2980	0.261	9.2981	0.8045	2.2298	2.2298
90	6.3976	0.261	10.4093	0.5535	2.3427	1.8559
120	4.6388	0.261	11.0832	0.4013	2.4054	1.5345
150	3.3994	0.261	11.5581	0.2941	2.4474	1.2236
180	3.4588	0.261	11.5353	0.2993	2.4454	1.2409
210	3.6353	0.261	11.4677	0.3145	2.4395	1.2907
240	3.5411	0.261	11.5038	0.3064	2.4427	1.2645
270	3.4424	0.261	11.5416	0.2978	2.4460	1.2362
300	3.4565	0.261	11.5362	0.2991	2.4455	1.2402

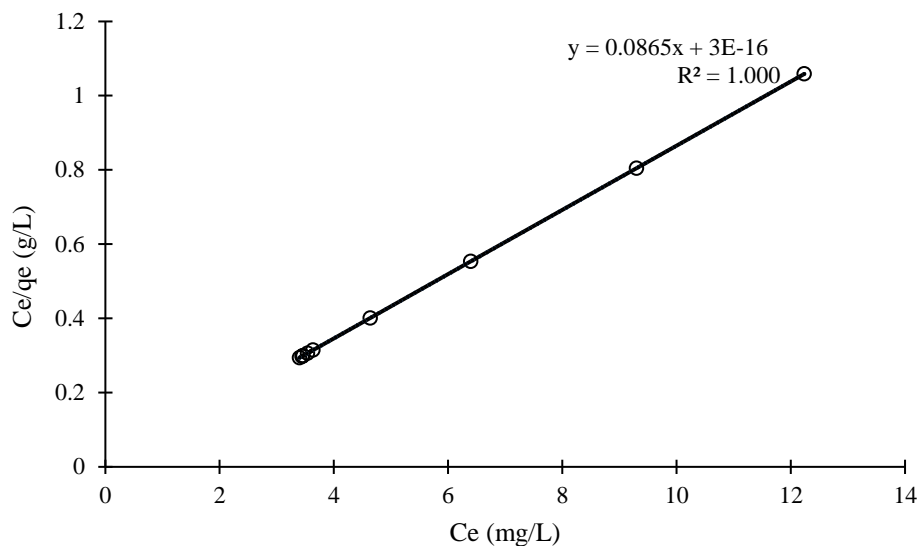


Figure 4.13: Langmuir Isotherm Plot for Adsorption of Congo Red.

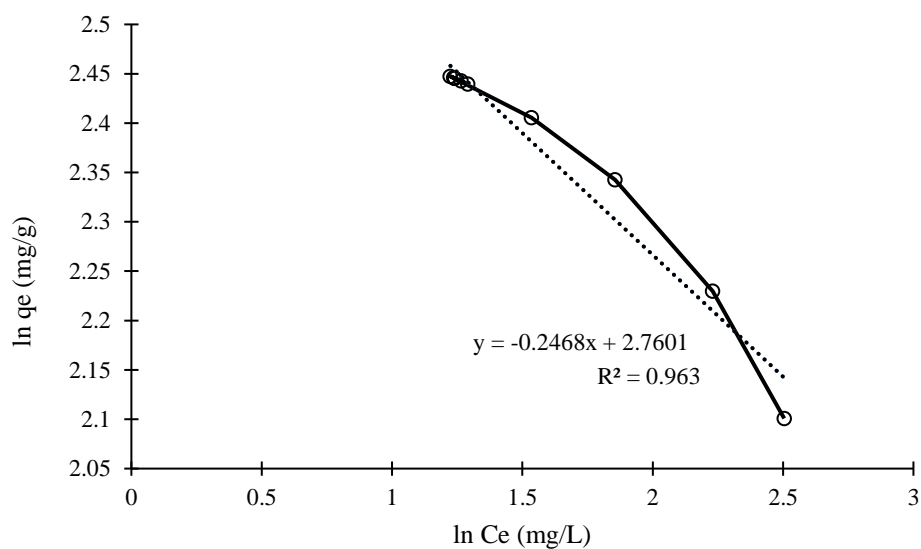


Figure 4.14: Freundlich Isotherm Plot for Adsorption of Congo Red.

Table 4.8: Parameters and Constants for Isotherm Modelling.

Model	k_L (L/mg)	q_0 (mg/g)	R_L	b (L/mg)
Langmuir	2.88×10^{14}	11.5607	1.033×10^{-16}	-
Freundlich	-	-	-	15.8014

4.4 Comparison of Various Adsorbents

The adsorption efficiency of PAC/PUF was compared to PUF and PAC adsorptions under constant pH of 3.854 and initial concentration of dye of 33.566 mg/L as shown in Figure 4.15. The highest adsorption efficiency of CR by PUF was observed at 57.60 %. Coating of PAC onto PUF indeed improved the removal efficiency to 89.86 %. This result was in line with another study whereby the adsorption of Methylene Blue only achieved approximately 70 % using non-coated PUF but increased in adsorption efficiency to 99 % when using PUF coated with PAC (Lefebvre et al., 2017). The possible reason for their higher adsorption efficiency of 70 %, compared to the result obtained in this study can be attributed to the utilization of different dyes and varying adsorption conditions during experiments.

Moreover, PAC/PUF showed higher adsorption efficiency than PAC adsorption, which achieved only 84.39 % efficiency at equilibrium within 150 min. It could be attributed to the highly porous PUF support which provided a large surface area for the adsorption of CR onto the PAC/PUF surface (Swain et al., 2021). Thus, PAC/PUF was proven to be a feasible adsorbent for removing CR.

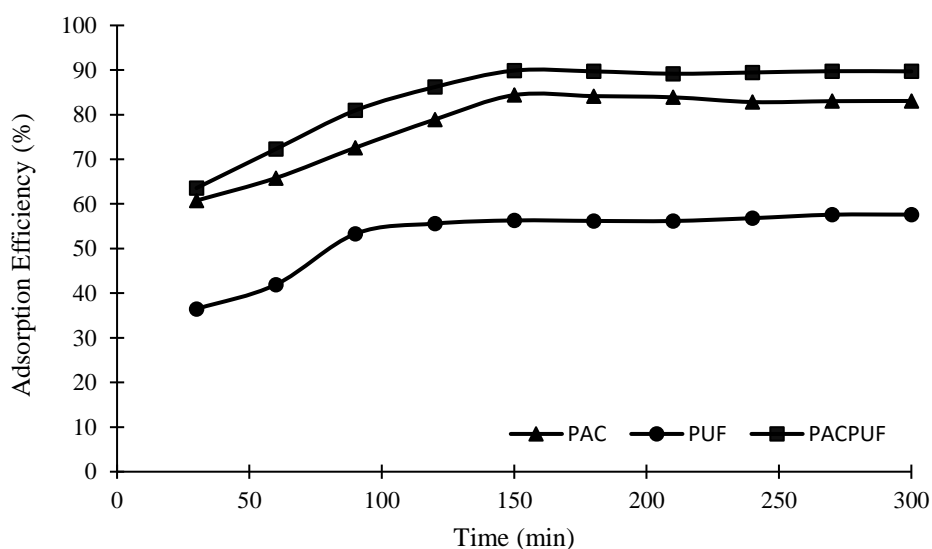


Figure 4.15: Adsorption Efficiency by Various Adsorbents.

CHAPTER 5

CONCLUSIONS AND RECOMMENDATIONS

5.1 Conclusions

In this study, PAC/PUF was used as a novel adsorbent to adsorb CR from a synthetic aqueous solution. Several characterization analyses, such as SEM-EDX, XRD, and FTIR had proven the successful loading of CR onto the surface of PAC/PUF during the adsorption experiments. SEM-EDX results of blank PUF portrayed smooth and highly porous network structures shaped like dodecahedrons cavities. These structures had plenty of micropores, allowing a high dye adsorption capacity. The images of PAC coated onto PUF also showed a significant morphological change whereby a rougher surface of PUF was obtained due to the distribution of highly dense PAC on its surfaces. This addition has helped the adsorbent to improve its adsorption capacity. The EDX results further proved the successful dye adsorption onto PAC/PUF.

Besides, XRD and FTIR results pointed out that all the characteristic peaks of CR could be found in the synthesized PAC/PUF, suggesting the effective adsorption of CR onto the adsorbent. For instance, the diffraction peaks at 2θ of $37^\circ - 45^\circ$ after adsorption experiments were intensified compared to before adsorption. Furthermore, XRD results showed that the adsorbent was amorphous. In addition, the point of zero charge analysis proved that the surface charges of PAC/PUF will change under acidic and alkaline conditions. This explained the favourable adsorption of CR when PAC/PUF was under an acidic dye solution.

The RSM was utilized to optimize the process variables, which included the pH, contact time, and initial concentration of dye. The optimum adsorption efficiency achieved was 89.86 % at pH of 3.854, contact time within 137.55 min, and an initial concentration of dye of 33.566 mg/L. The interactions between these parameters on the adsorption efficiency of CR were also studied using the response surface plots. It could be found that contact time had the most significant impact on the adsorption efficiency of CR. Apart from that, the adsorption efficiency of CR was improved in acidic solutions, long contact time and a low initial concentration of dye. Besides, ANOVA

suggested that the experimental data were well-fitted to the quadratic model with a R^2 value of 0.9660.

The analysis of kinetics data suggested the PSO model was the most suitable kinetic model due to the high R^2 value of 0.9988. Moreover, the Langmuir isotherm model was the best-fitted model to describe CR adsorption, with a high R^2 value of 1.000. Based on the characterization and adsorption modelling analyses, the adsorption of CR on PAC/PUF is mainly attributed to the chemisorption interaction between the dye and the functional groups of PAC/PUF.

Furthermore, the adsorption efficiency of CR using PAC/PUF was the highest compared to PAC and blank PUF alone. In conclusion, PAC/PUF was successfully synthesized and characterized. The overall optimization results suggested that PAC/PUF is a feasible adsorbent to remove CR from synthetic aqueous solution.

5.2 Recommendations for Future Work

Some recommendations could be carried out in future work to improve its experimental quality. The recommendations are listed as follows:

- (i) Use the impregnation method to synthesize PAC/PUF instead of the dip-coating method to obtain higher-end qualities such as a stronger adsorbent and even coating.
- (ii) Use different activated carbon sources to replace the commercial activated carbon to compare their adsorption efficiency of Congo Red.
- (iii) Recommend using transmission electron microscopy (TEM) or field emission scanning electron microscopy (FE-SEM) to capture the image of Congo Red instead of SEM since Congo Red is a relatively small molecule in the order of nanometers.
- (iv) Perform other characterization works such as Thermogravimetric Analyse (TGA) to study the thermal stability of PAC/PUF.
- (v) Investigate the reusability of PAC/PUF by repeating the adsorption experiment using the same PAC/PUF.

- (vi) Perform application analysis using industrial wastewater containing dye to test the effectiveness of PAC/PUF on the industrial scale.

REFERENCES

- Abate, G.Y., Alene, A.N., Habte, A.T. and Getahun, D.M., 2020. Adsorptive removal of malachite green dye from aqueous solution onto activated carbon of *Catha edulis* stem as a low cost bio-adsorbent. *Environmental Systems Research*, 9(1).
- Abdulhameed, A.S., Firdaus Hum, N.N.M., Rangabhashiyam, S., Jawad, A.H., Wilson, L.D., Yaseen, Z.M., Al-Kahtani, A.A. and Alothman, Z.A., 2021. Statistical modeling and mechanistic pathway for methylene blue dye removal by high surface area and mesoporous grass-based activated carbon using K_2CO_3 activator. *Journal of Environmental Chemical Engineering*, 9(4), p.105530.
- Adam, O.E.-A.A., 2016. Removal of Resorcinol from Aqueous Solution by Activated Carbon: Isotherms, Thermodynamics and Kinetics. *American Chemical Science Journal*, 16(1), pp.1–13.
- Adeleke, O.A., Ismail, N., Latiff, A.A.A., Saphira, M.R., Daud, Z., Aziz, N.A.A., Ndah, M., Kumar, V., Al-Gheethi, A., Rosli, M.A., Hijab, M., Ahsan, A. and Ahsan, A., 2019. Locally Derived Activated Carbon From Domestic, Agricultural and Industrial Wastes for the Treatment of Palm Oil Mill Effluent. In: A. Ahsan and A.F. Ismail, eds. *Nanotechnology in Water and Wastewater Treatment: Theory and Applications*. Elsevier. pp.35–62.
- Ahmad, M.A., Siti Nurul, S.N.A., Choong, T.S.Y., Abdullah, A.H., Mastuli, M.S., Othman, N. and Jiman, N.N., 2019a. Green Flexible Polyurethane Foam as a Potent Support for Fe-Si Adsorbent. *Polymers*, [online] 11(12).
- Ahmad, M.A., Ahmed, N.B., Adegoke, K.A. and Bello, O.S., 2019b. Sorption studies of methyl red dye removal using lemon grass (*Cymbopogon citratus*). *Chemical Data Collections*, 22, p.100249.
- Ahmed, I., Hasan, Z., Lee, G., Lee, H.J. and Jung, S.H., 2022. Contribution of hydrogen bonding to liquid-phase adsorptive removal of hazardous organics with metal-organic framework-based materials. *Chemical Engineering Journal*, 430, p.132596.
- Ajenifuja, E., Ajao, J.A. and Ajayi, E.O.B., 2017. Equilibrium adsorption isotherm studies of Cu (II) and Co (II) in high concentration aqueous solutions on Ag-TiO₂-modified kaolinite ceramic adsorbents. *Applied Water Science*, [online] 7(5), pp.2279–2286.
- Akhtar, K., Khan, S.A., Khan, S.B. and Asiri, A.M., 2018. Scanning electron microscopy: Principle and applications in nanomaterials characterization. In: S.K. Sharma, ed. *Handbook of Materials Characterization*. [online] Springer International Publishing. pp.113–145.

- AlAbdulaal, T., Assiri, M.A., Mohammed, M.I., Zahran, H.Y., Harraz, F.A., Al-Assiri, M.S., Yahia, I.S. and Ibrahim, M.A., 2022. Photophysical and electronic properties of Congo red dye embedded in polyvinyl alcohol as an efficient laser optical limiter: enhancement of the electrical conductivity and dielectric properties. *Optical and Quantum Electronics*, [online] 54(12), pp.1–18.
- Alam, S., Khan, M.S., Bibi, W., Zekker, I., Burlakovs, J., Ghangrekar, M.M., Bhowmick, G.D., Kallistova, A., Pimenov, N. and Zahoor, M., 2021. Preparation of Activated Carbon from the Wood of *Paulownia tomentosa* as an Efficient Adsorbent for the Removal of Acid Red 4 and Methylene Blue Present in Wastewater. *Water*, [online] 13(11), p.1453.
- Alaqarbeh, M., 2021. Adsorption Phenomena: Definition, Mechanisms, and Adsorption Types: Short Review. *RHAZES: Green and Applied Chemistry*, [online] 13(0), pp.43–51.
- Alhogbi, B.G., Altayeb, S., Bahaidarah, E.A., Zawrah, M.F., Alhogbi, C., Altayeb, B.G., Bahaidarah, S., Zawrah, E.A., Wawrzkievicz, M. and Show, P.L., 2021. Removal of Anionic and Cationic Dyes from Wastewater Using Activated Carbon from Palm Tree Fiber Waste. *Processes*, [online] 9(3), p.416.
- Ali, Y.A.E.H., N'diaye, A.D., Fahmi, D., Kankou, M.S. and Stitou, M., 2021. Adsorption of Congo red from Aqueous Solution using *Typha australis* Leaves as a Low Cost adsorbent. *Journal of Environmental Treatment Techniques*, [online] 9(2), pp.534–539.
- Al-Tohamy, R., Ali, S.S., Li, F., Okasha, K.M., Mahmoud, Y.A.G., Elsamahy, T., Jiao, H., Fu, Y. and Sun, J., 2022. A critical review on the treatment of dye-containing wastewater: Ecotoxicological and health concerns of textile dyes and possible remediation approaches for environmental safety. *Ecotoxicology and Environmental Safety*, 231, p.113160.
- Alwi, R.S., Gopinathan, R., Bhowal, A. and Garlapati, C., 2020. Adsorption Characteristics of Activated Carbon for the Reclamation of Eosin Y and Indigo Carmine Colored Effluents and New Isotherm Model. *Molecules*, [online] 25(24), p.6014.
- Amin, M.T., Alazba, A.A. and Shafiq, M., 2017. Effective adsorption of methylene blue dye using activated carbon developed from the rosemary plant: isotherms and kinetic studies. *Desalination and Water Treatment*, [online], pp. 1-10.
- Asim, T., Mamoona, M., Tahir, A., Nisar, N., Ali, A. and Sheikh, A., 2019. Alumina as environmentally stable adsorbent for the removal of dyesul black dye from waste water. *Water Practice and Technology*, 14(1), pp.62–70.

Azari, A., Nabizadeh, R., Nasser, S., Mahvi, A.H. and Mesdaghinia, A.R., 2020. Comprehensive systematic review and meta-analysis of dyes adsorption by carbon-based adsorbent materials: Classification and analysis of last decade studies. *Chemosphere*, 250, p.126238.

Behera, S.K., Meena, H., Chakraborty, S. and Meikap, B.C., 2018. Application of response surface methodology (RSM) for optimization of leaching parameters for ash reduction from low-grade coal. *International Journal of Mining Science and Technology*, 28(4), pp.621–629.

Benkhaya, S., M'rabet, S. and el Harfi, A., 2020. A review on classifications, recent synthesis and applications of textile dyes. *Inorganic Chemistry Communications*, 115, p.107891.

Bilir, M.H., Sakalar, N., Acemioglu, B., Baran, E. and Alma, M.H., 2013. Sorption of remazol brilliant blue R onto polyurethane-type foam prepared from peanut shell. *Journal of Applied Polymer Science*, [online] 127(6), pp.4340–4351.

Bourai, M. El and Abdelghany, A., 2020. Sorption Features of Polyurethane Foam Functionalized with Salicylate for Chlorpyrifos: Equilibrium, Kinetic Models and Thermodynamic Studies. *Polymers 2020*, [online] 12(9), p.2036.

Brandt, M.J., Johnson, K.M., Elphinston, A.J. and Ratnayaka, D.D., 2017. Specialized and Advanced Water Treatment Processes. In: M.J. Brandt, K.M. Johnson, A.J. Elphinston and D.D. Ratnayaka, eds. *Twort's Water Supply*, 7th ed. Butterworth-Heinemann. pp.407–473.

Caddeo, S., Bairo, F., Ferreira, A.M., Sartori, S., Novajra, G., Ciardelli, G. and Vitale-Brovarone, C., 2015. Collagen/Polyurethane-Coated Bioactive Glass: Early Achievements towards the Modelling of Healthy and Osteoporotic Bone. *Key Engineering Materials*, [online] 631, pp.184–189.

Ceretta, M.B., Nercessian, D. and Wolski, E.A., 2021. Current Trends on Role of Biological Treatment in Integrated Treatment Technologies of Textile Wastewater. *Frontiers in Microbiology*, 12, p.518.

Chandanshive, V., Kadam, S., Rane, N., Jeon, B.H., Jadhav, J. and Govindwar, S., 2020. In situ textile wastewater treatment in high rate transpiration system furrows planted with aquatic macrophytes and floating phytobeds. *Chemosphere*, 252.

Chang, H., Quan, X., Zhong, N., Zhang, Z., Lu, C., Li, G., Cheng, Z. and Yang, L., 2018. High-efficiency nutrients reclamation from landfill leachate by microalgae *Chlorella vulgaris* in membrane photobioreactor for bio-lipid production. *Bioresource Technology*, 266, pp.374–381.

Chukwuemeka-Okorie, H.O., Ekuma, F.K., Akpomie, K.G., Nnaji, J.C. and Okerefor, A.G., 2021. Adsorption of tartrazine and sunset yellow anionic dyes onto activated carbon derived from cassava sievate biomass. *Applied Water Science*, [online] 11(2), pp.1–8.

Crawford, C.B. and Quinn, B., 2017. The interactions of microplastics and chemical pollutants. In: *Microplastic Pollutants*. Elsevier. pp.131–157.

Crini, G., Lichtfouse, E., Wilson, L.D. and Morin-Crini, N., 2019. Conventional and non-conventional adsorbents for wastewater treatment. *Environmental Chemistry Letters*, 17(1), pp.195–213.

Dacewicz, E. and Grzybowska-Pietras, J., 2021. Polyurethane Foams for Domestic Sewage Treatment. *Materials*, [online] 14(4), p.933.

Das, A., Bhattacharya, S., Panchanan, G., Navya, B.S. and Nambiar, P., 2016. Production, characterization and Congo red dye decolourizing efficiency of a laccase from *Pleurotus ostreatus* MTCC 142 cultivated on co-substrates of paddy straw and corn husk. *Journal of Genetic Engineering and Biotechnology*, 14(2), pp.281–288.

Department of Environment Malaysia, 2020. *Environmental Quality Report*. [online] Available at: <<https://enviro2.doe.gov.my/ekmc/wp-content/uploads/2021/09/EQR-2020-1.pdf>> [Accessed 18 February 2023].

Dias, R.C.M., Góes, A.M., Serakides, R., Ayres, E. and Oréfce, R.L., 2010. Porous biodegradable polyurethane nanocomposites: preparation, characterization, and biocompatibility tests. *Materials Research*, [online] 13(2), pp.211–218.

Dutrow, B.L. and Clark, C.M., 2019. *X-ray Powder Diffraction (XRD)*. [online] Available at: <https://serc.carleton.edu/research_education/geochemsheets/techniques/XRD.html> [Accessed 16 January 2023].

Dutta, S., Gupta, B., Srivastava, S.K. and Gupta, A.K., 2021. Recent advances on the removal of dyes from wastewater using various adsorbents: a critical review. *Materials Advances*, [online] 2(14), pp.4497–4531.

Elgarahy, A.M., Elwakeel, K.Z., Mohammad, S.H. and Elshoubaky, G.A., 2021. A critical review of biosorption of dyes, heavy metals and metalloids from wastewater as an efficient and green process. *Cleaner Engineering and Technology*, 4.

Ezugbe, E.O. and Rathilal, S., 2020. Membrane Technologies in Wastewater Treatment: A Review. *Membranes*, [online] 10(5), p.89.

Farhana, K., Shadate, A., Mahamude, F., Mushfika, . and Mica, T., 2022. The Scenario of Textile Industry in Malaysia: A Review for Potentiality. *Materials Circular Economy*, [online] 4(1), pp.1–15.

Fernandes, E.P., Silva, T.S., Carvalho, C.M., Selvasembian, R., Chaukura, N., Oliveira, L.M.T.M., Meneghetti, S.M.P. and Meili, L., 2021. Efficient adsorption of dyes by γ -alumina synthesized from aluminum wastes: Kinetics, isotherms, thermodynamics and toxicity assessment. *Journal of Environmental Chemical Engineering*, 9(5), p.106198.

Francés, A.B. and Bañón, M.V.N., 2014. Effect of silica nanoparticles on polyurethane foaming process and foam properties. *IOP Conference Series: Materials Science and Engineering*, [online] 64(1), p.012020.

Fröhlich, A.C., Foletto, E.L. and Dotto, G.L., 2019. Preparation and characterization of NiFe₂O₄/activated carbon composite as potential magnetic adsorbent for removal of ibuprofen and ketoprofen pharmaceuticals from aqueous solutions. *Journal of Cleaner Production*, 229, pp.828–837.

Gičević, A., Hindija, L. and Karačić, A., 2020. Toxicity of azo dyes in pharmaceutical industry. *IFMBE Proceedings*, 73, pp.581–587.

Harja, M., Buema, G. and Bucur, D., 2022. Recent advances in removal of Congo Red dye by adsorption using an industrial waste. *Scientific Reports*, [online] 12(1), pp.1–18.

Hassan, M.M. and Carr, C.M., 2018. A critical review on recent advancements of the removal of reactive dyes from dyehouse effluent by ion-exchange adsorbents. *Chemosphere*, 209, pp.201–219.

Hassan, S.S.M., Awwad, N.S. and Aboterika, A.H.A., 2009. Removal of synthetic reactive dyes from textile wastewater by Sorel's cement. *Journal of hazardous materials*, [online] 162(2–3), pp.994–999.

Hazman Hasan, H., Fatin Mohd Razali, S. and Shazali Mhd Shah, A., 2022. Performance of Greywater Treatment Using Iron Removal Media (IRM) and Cattail Typha Angustifolia. *Pertanika Journal of Science & Technology*, 30(2), pp.1421–1438.

Hernández-Zamora, M. and Martínez-Jerónimo, F., 2019. Congo red dye diversely affects organisms of different trophic levels: a comparative study with microalgae, cladocerans, and zebrafish embryos. *Environmental Science and Pollution Research*, 26(12), pp.11743–11755.

Hussain, B., Yaseen, H., Khalid-Al-Ghanim, Al-Misned, F., Qasim, M., Al-Mulhm, N. and Mahboob, S., 2021. A study on risk assessment of effect of hematoxylin dye on cytotoxicity and nephrotoxicity in freshwater fish: Food and water security prospective research. *Saudi Journal of Biological Sciences*, 28(4), pp.2267–2271.

Imessaoudene, A., Cheikh, S., Bollinger, J.-C., Belkhiri, L., Tiri, A., Bouzaza, A., Jery, A. el, Assadi, A., Amrane, A. and Mouni, L., 2022. Zeolite Waste Characterization and Use as Low-Cost, Ecofriendly, and Sustainable Material for Malachite Green and Methylene Blue Dyes Removal: Box-Behnken Design, Kinetics, and Thermodynamics. *Applied Sciences*, [online] 12(15), p.7587.

Jamee, R. and Siddique, R., 2019. Biodegradation of Synthetic Dyes of Textile Effluent by Microorganisms: An Environmentally and Economically Sustainable Approach. *European Journal of Microbiology & Immunology*, [online] 9(4), p.114.

Jawad, A.H. and Abdulhameed, A.S., 2020. Statistical modeling of methylene blue dye adsorption by high surface area mesoporous activated carbon from bamboo chip using KOH-assisted thermal activation. *Energy, Ecology and Environment*, 5(6), pp.456–469.

Kajjumba, G.W., Emik, S., Öngen, A., Aydın, H.K.Ö. and S., Kajjumba, G.W., Emik, S., Öngen, A. and Aydın, H.K.Ö. and S., 2018. Modelling of Adsorption Kinetic Processes—Errors, Theory and Application. In: S. Edebali, ed. *Advanced Sorption Process Applications*. [online] IntechOpen.

Katheresan, V., Kansedo, J. and Lau, S.Y., 2018. Efficiency of various recent wastewater dye removal methods: A review. *Journal of Environmental Chemical Engineering*, 6(4), pp.4676–4697.

Keshavarz, A., Zilouei, H., Abdolmaleki, A., Asadinezhad, A. and Nikkhah, A.A., 2016. Impregnation of polyurethane foam with activated carbon for enhancing oil removal from water. *International Journal of Environmental Science and Technology*, 13(2), pp.699–710.

Kishor, R., Purchase, D., Saratale, G.D., Saratale, R.G., Ferreira, L.F.R., Bilal, M., Chandra, R. and Bharagava, R.N., 2021. Ecotoxicological and health concerns of persistent coloring pollutants of textile industry wastewater and treatment approaches for environmental safety. *Journal of Environmental Chemical Engineering*, 9(2), p.105012.

Kittappa, S., Jais, F.M., Ramalingam, M. and Ibrahim, S., 2020. Functionalized magnetic mesoporous palm shell activated carbon for enhanced removal of azo dyes. *Journal of Environmental Chemical Engineering*, 8(5), p.104081.

Kraitape, N. and Thongpin, C., 2016. Influence of Recycled Polyurethane Polyol on the Properties of Flexible Polyurethane Foams. *Energy Procedia*, 89, pp.186–197.

Kuang, Y., Zhang, X. and Zhou, S., 2020. Adsorption of Methylene Blue in Water onto Activated Carbon by Surfactant Modification. *Water*, [online] 12(2), p.587.

Kumar, A., Dixit, U., Singh, K., Gupta, S.P., Beg, M.S.J., Kumar, A., Dixit, U., Singh, K., Gupta, S.P. and Beg, M.S.J., 2021. Structure and Properties of Dyes and Pigments. In: P. Raffaello, ed. *Dyes and Pigments - Novel Applications and Waste Treatment*. [online] IntechOpen.

Kumari, M. and Gupta, S.K., 2019. Response surface methodological (RSM) approach for optimizing the removal of trihalomethanes (THMs) and its precursor's by surfactant modified magnetic nanoadsorbents (sMNP) - An endeavor to diminish probable cancer risk. *Scientific Reports*, [online] 9(1), pp.1–11.

Lafi, R., Montasser, I. and Hafiane, A., 2019. Adsorption of congo red dye from aqueous solutions by prepared activated carbon with oxygen-containing functional groups and its regeneration. *Adsorption Science and Technology*, [online] 37(1–2), pp.160–181.

Laksmono, J.A., Pangesti, U.A., Sudibandriyo, M., Haryono, A. and Saputra, A.H., 2018. Adsorption capacity study of ethanol-water mixture for zeolite, activated carbon, and polyvinyl alcohol. In: *IOP Conference Series: Earth and Environmental Science*. [online] IOP Publishing.

Latinwo, G.K., Alade, A.O., Agarry, S.E. and Dada, E.O., 2019. Process Optimization and Modeling the Adsorption of Polycyclic Aromatic-Congo Red Dye onto Delonix regia Pod-Derived Activated Carbon. *Polycyclic Aromatic Compounds*, [online] 41(2), pp.400–418.

Lee, W., Yoon, S., Choe, J.K., Lee, M. and Choi, Y., 2018. Anionic surfactant modification of activated carbon for enhancing adsorption of ammonium ion from aqueous solution. *Science of The Total Environment*, 639, pp.1432–1439.

Lefebvre, L., Agusti, G., Bouzegane, A. and Edouard, D., 2018. Adsorption of dye with carbon media supported on polyurethane open cell foam. *Catalysis Today*, 301, pp.98–103.

Lefebvre, L., Kelber, J., Jierry, L., Ritleng, V. and Edouard, D., 2017. Polydopamine-coated open cell polyurethane foam as an efficient and easy-to-regenerate soft structured catalytic support (S₂CS) for the reduction of dye. *Journal of Environmental Chemical Engineering*, 5(1), pp.79–85.

Li, J., Xu, C., Zhang, Y., Wang, R., Zha, F. and She, H., 2016. Robust superhydrophobic attapulgite coated polyurethane sponge for efficient immiscible oil/water mixture and emulsion separation. *Journal of Materials Chemistry A*, [online] 4(40), pp.15546–15553.

Li, Z., Hanafy, H., Zhang, L., Sellaoui, L., Schadeck Netto, M., Oliveira, M.L.S., Seliem, M.K., Luiz Dotto, G., Bonilla-Petriciolet, A. and Li, Q., 2020. Adsorption of congo red and methylene blue dyes on an ashitaba waste and a walnut shell-based activated carbon from aqueous solutions: Experiments, characterization and physical interpretations. *Chemical Engineering Journal*, 388, p.124263.

Lim, S., Kim, J.H., Park, H., Kwak, C., Yang, J., Kim, J., Ryu, S.Y. and Lee, J., 2021. Role of electrostatic interactions in the adsorption of dye molecules by Ti_3C_2 -MXenes. *RSC Advances*, [online] 11(11), pp.6201–6211.

Liu, H., Dong, M., Huang, W., Gao, J., Dai, K., Guo, J., Zheng, G., Liu, C., Shen, C. and Guo, Z., 2016. Lightweight conductive graphene/thermoplastic polyurethane foams with ultrahigh compressibility for piezoresistive sensing. *Journal of Materials Chemistry C*, [online] 5(1), pp.73–83.

Liu, L., Luo, X.B., Ding, L. and Luo, S.L., 2019. Application of Nanotechnology in the Removal of Heavy Metal From Water. In: X. Luo and F. Deng, eds. *Nanomaterials for the Removal of Pollutants and Resource Reutilization*. Elsevier. pp.83–147.

Ma, M., Ying, H., Cao, F., Wang, Q. and Ai, N., 2020. Adsorption of congo red on mesoporous activated carbon prepared by CO_2 physical activation. *Chinese Journal of Chemical Engineering*, 28(4), pp.1069–1076.

Ma, Y., Zhang, X. and Wen, J., 2021. Study on the Harm of Waste Activated Carbon and Novel Regeneration Technology of it . *IOP Conference Series: Earth and Environment Science* , 769, p.22047.

Machdar, I., Onodera, T., Syutsubo, K. and Ohashi, A., 2018. Effects of sponge pore-size on the performance of a down-flow hanging sponge reactor in post-treatment of effluent from an anaerobic reactor treating domestic wastewater. *Sustainable Environment Research*, 28(6), pp.282–288.

Maheshwari, K., Agrawal, M. and Gupta, A.B., 2021. Dye Pollution in Water and Wastewater. In: S.S. Muthu and A. Khadir, eds. *Novel Materials for Dye-containing Wastewater Treatment*. [online] Springer, Singapore. pp.1–25.

Mailler, R., Gasperi, J., Coquet, Y., Derome, C., Buleté, A., Vulliet, E., Bressy, A., Varrault, G., Chebbo, G. and Rocher, V., 2016. Removal of emerging micropollutants from wastewater by activated carbon adsorption: Experimental study of different activated carbons and factors influencing the adsorption of micropollutants in wastewater. *Journal of Environmental Chemical Engineering*, 4(1), pp.1102–1109.

Mallakpour, S. and Behranvand, V., 2020. Modification of polyurethane sponge with waste compact disc-derived activated carbon and its application in organic solvents/oil sorption. *New Journal of Chemistry*, 44(36), pp.15609–15616.

Mallakpour, S. and Behranvand, V., 2021. Polyurethane sponge modified by alginate and activated carbon with abilities of oil absorption, and selective cationic and anionic dyes clean-up. *Journal of Cleaner Production*, 312, p.127513.

el Malti, W., Hamieh, M., Noaman, A., El-Dine, R.N., Hijazi, A. and Al-Khatib, W., 2021. Polyurethane Loaded with Vegetable Activated Carbon for Heavy Metals Removal from Water. *Journal of Ecological Engineering*, [online] 22(9), pp.99–110.

Mandal, S., Calderon, J., Marpu, S.B., Omary, M.A. and Shi, S.Q., 2021. Mesoporous activated carbon as a green adsorbent for the removal of heavy metals and Congo red: Characterization, adsorption kinetics, and isotherm studies. *Journal of Contaminant Hydrology*, 243, p.103869.

Masoudian, N., Rajabi, M. and Ghaedi, M., 2019. Titanium oxide nanoparticles loaded onto activated carbon prepared from bio-waste watermelon rind for the efficient ultrasonic-assisted adsorption of congo red and phenol red dyes from wastewaters. *Polyhedron*, 173, p.114105.

Mohamed, M.A., Jaafar, J., Ismail, A.F., Othman, M.H.D. and Rahman, M.A., 2017. Fourier Transform Infrared (FTIR) Spectroscopy. In: N. Hilal, A.F. Ismail, T. Matsuura and D. Oatley-Radcliffe, eds. *Membrane Characterization*. Elsevier. pp.3–29.

Moon, S.A., Salunke, B.K., Saha, P., Deshmukh, A.R. and Kim, B.S., 2018. Comparison of dye degradation potential of biosynthesized copper oxide, manganese dioxide, and silver nanoparticles using *Kalopanax pictus* plant extract. *Korean Journal of Chemical Engineering*, [online] 35(3), pp.702–708.

Moosavi, S., Lai, C.W., Gan, S., Zamiri, G., Akbarzadeh Pivehzhani, O. and Johan, M.R., 2020. Application of efficient magnetic particles and activated carbon for dye removal from wastewater. *ACS Omega*, [online] 5(33), pp.20684–20697.

Natarajan, S., Bajaj, H.C. and Tayade, R.J., 2018. Recent advances based on the synergetic effect of adsorption for removal of dyes from waste water using photocatalytic process. *Journal of Environmental Sciences*, 65, pp.201–222.

Nizam, N.U.M., Hanafiah, M.M., Mahmoudi, E., Halim, A.A. and Mohammad, A.W., 2021. The removal of anionic and cationic dyes from an aqueous solution using biomass-based activated carbon. *Scientific Reports*, [online] 11(1), pp.1–17.

Omri, A. and Benzina, M., 2012. CHARACTERIZATION OF ACTIVATED CARBON PREPARED FROM A NEW RAW LIGNOCELLULOSIC MATERIAL: ZIZIPHUS SPINA-CHRISTI SEEDS. *Journal de la Société Chimique de Tunisie*, 14, pp.175–183.

Patra, A.S., Ghorai, S., Sarkar, D., Das, R., Sarkar, S. and Pal, S., 2017. Anionically functionalized guar gum embedded with silica nanoparticles: An efficient nanocomposite adsorbent for rapid adsorptive removal of toxic cationic dyes and metal ions. *Bioresource Technology*, 225, pp.367–376.

Patra, C., Gupta, R., Bedadeep, D. and Narayanasamy, S., 2020. Surface treated acid-activated carbon for adsorption of anionic azo dyes from single and binary adsorptive systems: A detail insight. *Environmental Pollution*, 266, p.115102.

Van Pham, T., Van Tran, T., Duy Nguyen, T., Thi Hong Tham, N., Thanh Tri Quang, P., Thi To Uyen, D., Thi Hong Le, N., Vo, D.V.N., Trung Thanh, N. and Giang Bach, L., 2019. Development of Response Surface Methodology for Optimization of Congo Red Adsorption Utilizing Exfoliated Graphite As An Efficient Adsorbent. *Materials Today: Proceedings*, 22, pp.2341–2350.

Piri, F., Mollahosseini, A., Khadir, A. and Milani Hosseini, M., 2019. Enhanced adsorption of dyes on microwave-assisted synthesized magnetic zeolite-hydroxyapatite nanocomposite. *Journal of Environmental Chemical Engineering*, 7(5), p.103338.

Pourhakkak, P., Taghizadeh, M., Taghizadeh, A. and Ghaedi, M., 2021. Adsorbent. In: M. Ghaedi, ed. *Interface Science and Technology*. Elsevier. pp.71–210.

Prashantha Kumar, T.K.M., Mandlimath, T.R., Sangeetha, P., Sakthivel, P., Revathi, S.K., Ashok Kumar, S.K. and Sahoo, S.K., 2015. Highly efficient performance of activated carbon impregnated with Ag, ZnO and Ag/ZnO nanoparticles as antimicrobial materials. *RSC Advances*, [online] 5(130), pp.108034–108043.

PubChem, 2023. *Congo red* . [online] National Center for Biotechnology Information. Available at: <<https://pubchem.ncbi.nlm.nih.gov/compound/Congo-red#section=Chemical-and-Physical-Properties>> [Accessed 18 January 2023].

Quesada, H.B., de Araújo, T.P., Cusioli, L.F., de Barros, M.A.S.D., Gomes, R.G. and Bergamasco, R., 2022. Caffeine removal by chitosan/activated carbon composite beads: Adsorption in tap water and synthetic hospital wastewater. *Chemical Engineering Research and Design*, 184, pp.1–12.

Rafaqat, S., Ali, N., Torres, C. and Rittmann, B., 2022. Recent progress in treatment of dyes wastewater using microbial-electro-Fenton technology. *RSC Advances*, [online] 12(27), p.17137.

Rajoriya, S., Saharan, V.K., Pundir, A.S., Nigam, M. and Roy, K., 2021. Adsorption of methyl red dye from aqueous solution onto eggshell waste material: Kinetics, isotherms and thermodynamic studies. *Current Research in Green and Sustainable Chemistry*, 4, p.100180.

Ramezani, H., Azizi, S.N. and Hosseini, S.R., 2017. NaY zeolite as a platform for preparation of Ag nanoparticles arrays in order to construction of H₂O₂ sensor. *Sensors and Actuators B: Chemical*, 248, pp.571–579.

- Rastegarfar, N., Behrooz, R. and Barikani, M., 2018. Characterization of polyurethane foams prepared from liquefied sawdust by crude glycerol and polyethylene glycol. *Journal of Polymer Research*, [online] 25(7), pp.1–8.
- Raval, N., Maheshwari, R., Kalyane, D., Youngren-Ortiz, S.R., Chougule, M.B. and Tekade, R.K., 2019. Importance of Physicochemical Characterization of Nanoparticles in Pharmaceutical Product Development. In: R.K. Tekade, ed. *Basic Fundamentals of Drug Delivery*. Academic Press. pp.369–400.
- Rawat, D., Sharma, R.S., Karmakar, S., Arora, L.S. and Mishra, V., 2018. Ecotoxic potential of a presumably non-toxic azo dye. *Ecotoxicology and Environmental Safety*, 148, pp.528–537.
- Revellame, E.D., Fortela, D.L., Sharp, W., Hernandez, R. and Zappi, M.E., 2020. Adsorption kinetic modeling using pseudo-first order and pseudo-second order rate laws: A review. *Cleaner Engineering and Technology*, 1, p.100032.
- Riyanti, F., Hariani, P.L., Purwaningrum, W., Elfita, E., Damarril, S.S. and Amelia, I., 2018. The Synthesis of MnFe₂O₄-Activated Carbon Composite for Removal of Methyl Red From Aqueous Solution. *Molekul*, [online] 13(2), pp.123–132.
- Roy, M. and Saha, R., 2021. Dyes and their removal technologies from wastewater: A critical review. In: S. Bhattacharyya, J. Platos, P. Krömer, N.K. Mondal and V. Snášel, eds. *Intelligent Environmental Data Monitoring for Pollution Management*. Academic Press. pp.127–160.
- Sahoo, T.R. and Prelot, B., 2020. Adsorption processes for the removal of contaminants from wastewater: the perspective role of nanomaterials and nanotechnology. In: B. Bonelli, F.S. Freyria, I. Rossetti and R. Sethi, eds. *Nanomaterials for the Detection and Removal of Wastewater Pollutants*. Elsevier. pp.161–222.
- Saleem, J., Shahid, U. bin, Hijab, M., Mackey, H. and McKay, G., 2019. Production and applications of activated carbons as adsorbents from olive stones. *Biomass Conversion and Biorefinery*, [online] 9(4), pp.775–802.
- San, V., Spoann, V. and Schmidt, J., 2018. Industrial pollution load assessment in Phnom Penh, Cambodia using an industrial pollution projection system. *Science of The Total Environment*, 615, pp.990–999.
- Sarayu, K. and Sandhya, S., 2012. Current technologies for biological treatment of textile wastewater-A review. *Applied Biochemistry and Biotechnology*, [online] 167(3), pp.645–661.

Sarkar, S., Banerjee, A., Halder, U., Biswas, R. and Bandopadhyay, R., 2017. Degradation of Synthetic Azo Dyes of Textile Industry: A Sustainable Approach Using Microbial Enzymes. *Water Conservation Science and Engineering*, [online] 2(4), pp.121–131.

Sayem, A., Ahmed, F., Saha, P. and Talukder, B., 2021. A Review on Natural Dyes: Raw Materials, Extraction Process, and their Properties. *Advance Research in Textile Engineering*, [online] 6(1). Available at: <www.austinpublishinggroup.com> [Accessed 16 January 2023].

Senthil Kumar, P., Joshiba, G.J., Femina, C.C., Varshini, P., Priyadharshini, S., Karthick, A. and Jothirani, R., 2019. A critical review on recent developments in the low-cost adsorption of dyes from wastewater. *Desalination and Water Treatment*, [online] 172, pp.395–416.

Sharaf, A. and Liu, Y., 2021. Mechanisms and kinetics of greywater treatment using biologically active granular activated carbon. *Chemosphere*, 263, p.128113.

Sharma, M., Joshi, M., Nigam, S., Shree, S., Avasthi, D.K., Adelong, R., Srivastava, S.K. and Kumar Mishra, Y., 2019. ZnO tetrapods and activated carbon based hybrid composite: Adsorbents for enhanced decontamination of hexavalent chromium from aqueous solution. *Chemical Engineering Journal*, 358, pp.540–551.

Shivaprasad, P., Kaushik, S., Sivasamy, A. and Nethaji, S., 2019. Superparamagnetic nanocomposites derived from waste polyurethane foam for the removal of Rhodamine B: batch and continuous column studies. *Separation Science and Technology*, [online] 55(16), pp.2879–2889.

Sid, N. and El-Hawary, S., 2019. High-Performance Natural Dyes for Cellulosic Fibers Review - part 1. *Journal of Textiles, Coloration and Polymer Science*, [online] 16(1), pp.1–13.

Siddiqui, S.I., Allehyani, E.S., Al-Harbi, S.A., Hasan, Z., Abomuti, M.A., Rajor, H.K. and Oh, S., 2023. Investigation of Congo Red Toxicity towards Different Living Organisms: A Review. *Processes*, [online] 11(3), p.807.

Singh, R. and Srivastava, S., 2017. A critical review on extraction of natural dyes from leaves. *International Journal of Home Science*, [online] 3(2), pp.100–103. Available at: <www.homesciencejournal.com> [Accessed 16 January 2023].

Singh, S., Wasewar, K.L. and Kansal, S.K., 2020. Low-cost adsorbents for removal of inorganic impurities from wastewater. In: P. Devi, P. Singh and S.K. Kansal, eds. *Inorganic Pollutants in Water*. Elsevier. pp.173–203.

Singh, V.P., Sharma, M. and Vaish, R., 2019. Separation of dyes/oils from water by diesel exhaust emission soot coated polyurethane foam: a kinetic and equilibrium isotherm study. *Engineering Research Express*, [online] 1(1), p.015010.

Singh, V.P. and Vaish, R., 2019. Candle soot coated polyurethane foam as an adsorbent for removal of organic pollutants from water. *The European Physical Journal Plus*, [online] 134(9), pp.1–10.

Siyal, A.A., Shamsuddin, M.R., Low, A. and Rabat, N.E., 2020. A review on recent developments in the adsorption of surfactants from wastewater. *Journal of Environmental Management*, 254.

Sohbatzadeh, H., Keshtkar, A.R., Safdari, J. and Fatemi, F., 2016. U(VI) biosorption by bi-functionalized *Pseudomonas putida* @ chitosan bead: Modeling and optimization using RSM. *International journal of biological macromolecules*, [online] 89, pp.647–658.

Swain, G., Singh, S., Sonwani, R.K., Singh, R.S., Jaiswal, R.P. and Rai, B.N., 2021. Removal of Acid Orange 7 dye in a packed bed bioreactor: Process optimization using response surface methodology and kinetic study. *Bioresource Technology Reports*, 13, p.100620.

Tadda, M.A., Ahsan, A., Shitu, A., ElSergany, M., Arunkumar, T., Jose, B., Razzaque, M.A. and Nik Daud, N.N., 2016. A Review on Activated Carbon: Process, Application and Prospects. *Journal of Advanced Civil Engineering Practice and Research*, [online] 2(1), pp.7–13. Available at: <https://www.researchgate.net/publication/308207482_A_Review_on_Activated_Carbon_Process_Application_and_Prospects> [Accessed 18 January 2023].

Temel, F., Turkyilmaz, M. and Kucukcongar, S., 2020. Removal of methylene blue from aqueous solutions by silica gel supported calix[4]arene cage: Investigation of adsorption properties. *European Polymer Journal*, 125, p.109540.

Terrazas, K.A.A., Nahúm, M.-C., Baltazar, Á. de J.R., Pérez, O.T. and López, S.Y.R., 2021. REVIEW OF ALUMINA IN ADSORPTION PROCESSES FOR EMERGING POLLUTANTS. *International Journal of Research - GRANTHAALAYAH*, 9(4), pp.435–453.

Thanavel, M., Kadam, S.K., Biradar, S.P., Govindwar, S.P., Jeon, B.H. and Sadasivam, S.K., 2019. Combined biological and advanced oxidation process for decolorization of textile dyes. *SN Applied Sciences*, [online] 1(1), pp.1–16.

Tran, H.N., Wang, Y.F., You, S.J. and Chao, H.P., 2017. Insights into the mechanism of cationic dye adsorption on activated charcoal: The importance of π - π interactions. *Process Safety and Environmental Protection*, 107, pp.168–180.

- Tripathi, M., Kumar, S., Singh, D.N., Pandey, R., Pathak, N. and Fatima, H., 2021. Bioremediation of Dye Contaminated Soil. In: J.A. Parray, A.H.A.E. Mahmoud and R. Sayyed, eds. *Soil Bioremediation*. [online] John Wiley & Sons, Ltd. pp.115–142.
- Udayakumar, M., Boros, R.Z., Farkas, L., Simon, A., Koós, T., Leskó, M., Leskó, A.K., Hernadi, K. and Németh, Z., 2021a. Composite Carbon Foams as an Alternative to the Conventional Biomass-Derived Activated Carbon in Catalytic Application. *Materials*, [online] 14(16), p.4540.
- Udayakumar, M., el Mrabate, B., Koós, T., Szemmelveisz, K., Kristály, F., Leskó, M., Filep, Á., Géber, R., Schabikowski, M., Baumli, P., Lakatos, J., Tóth, P. and Németh, Z., 2021b. Synthesis of activated carbon foams with high specific surface area using polyurethane elastomer templates for effective removal of methylene blue. *Arabian Journal of Chemistry*, 14(7), p.103214.
- Uddin, M.K. and Nasar, A., 2020. Walnut shell powder as a low-cost adsorbent for methylene blue dye: isotherm, kinetics, thermodynamic, desorption and response surface methodology examinations. *Scientific Reports*, [online] 10(1), pp.1–13.
- Varjani, S., Rakholiya, P., Ng, H.Y., You, S. and Teixeira, J.A., 2020. Microbial degradation of dyes: An overview. *Bioresource Technology*, 314.
- Wang, J. and Guo, X., 2020. Adsorption isotherm models: Classification, physical meaning, application and solving method. *Chemosphere*, [online] 258, p.127279.
- Wang, J., Ma, J. and Sun, Y., 2022. Adsorption of Methylene Blue by Coal-Based Activated Carbon in High-Salt Wastewater. *Water*, [online] 14(21), p.3576.
- Wu, D., Fang, L., Qin, Y., Wu, W., Mao, C. and Zhu, H., 2014. Oil sorbents with high sorption capacity, oil/water selectivity and reusability for oil spill cleanup. *Marine pollution bulletin*, [online] 84(1–2), pp.263–267.
- Wu, J., Li, Q., Li, W., Li, Y., Wang, G., Li, A. and Li, H., 2020. Efficient removal of acid dyes using permanent magnetic resin and its preliminary investigation for advanced treatment of dyeing effluents. *Journal of Cleaner Production*, 251, p.119694.
- Wu, L., Xie, Q., Lv, Y., Zhang, Z., Wu, Z., Liang, X., Lu, M. and Nie, Y., 2019. Degradation of methylene blue by dielectric barrier discharge plasma coupled with activated carbon supported on polyurethane foam. *RSC Advances*, 9(45), pp.25967–25975.
- Yang, H.C., Gong, J.L., Zeng, G.M., Zhang, P., Zhang, J., Liu, H.Y. and Huan, S.Y., 2017. Polyurethane foam membranes filled with humic acid-chitosan crosslinked gels for selective and simultaneous removal of dyes. *Journal of Colloid and Interface Science*, 505, pp.67–78.

Yuan, D., Zhang, T., Guo, Q., Qiu, F., Yang, D. and Ou, Z., 2017. A novel hierarchical hollow $\text{SiO}_2@\text{MnO}_2$ cubes reinforced elastic polyurethane foam for the highly efficient removal of oil from water. *Chemical Engineering Journal*, 327, pp.539–547.

Yusuff, A.S., 2019. Adsorption of hexavalent chromium from aqueous solution by *Leucaena leucocephala* seed pod activated carbon: equilibrium, kinetic and thermodynamic studies. *Arab Journal of Basic and Applied Sciences*, [online] 26(1), pp.89–102.

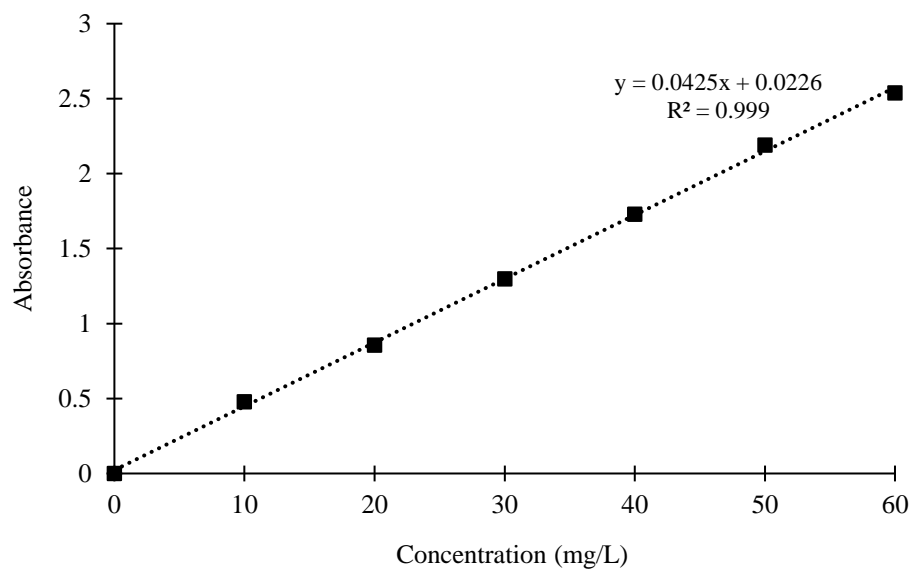
Zhang, L., Song, F., Wang, S., Wang, H., Yang, W. and Li, Y., 2020. Efficient Removal of Hexavalent Chromium and Congo Red by Graphene Oxide/Silica Nanosheets with Multistage Pores. *Journal of Chemical and Engineering Data*, [online] 65(9), pp.4354–4368.

Zhang, Y., Xia, K., Liu, X., Chen, Z., Du, H. and Zhang, X., 2019. Synthesis of cationic-modified silica gel and its adsorption properties for anionic dyes. *Journal of the Taiwan Institute of Chemical Engineers*, 102, pp.1–8.

Zhao, J., Xu, L., Su, Y., Yu, H., Liu, H., Qian, S., Zheng, W. and Zhao, Y., 2021. Zr-MOFs loaded on polyurethane foam by polydopamine for enhanced dye adsorption. *Journal of Environmental Sciences*, 101, pp.177–188.

APPENDICES

Appendix A: Standard Calibration Curve of Congo Red



Graph A-1: Calibration Curve of Congo Red Solution